

Emergent conservation in atmospheric chemical mechanisms

Beatriz Lucia G. Rodriguez^{1†}, Patrick Obin Sturm^{1†}, Daniel Getter¹, and Sam J. Silva^{1,2,3}

¹Department of Earth Sciences, University of Southern California, Los Angeles, CA, USA

²Department of Environmental Engineering, University of Southern California, Los Angeles, CA, USA

³Department of Population and Public Health Sciences, University of Southern California, Los Angeles, CA, USA

Corresponding author: Patrick Obin Sturm (psturm@usc.edu)

†Equally contributing authors

Key Points:

- Widely used atmospheric chemical mechanisms contain emergent conservation laws that reduce their dimensionality
- This emergent conservation behavior is independent of mass conservation, arising from coupled kinetics in the mechanism
- We survey 35 chemical mechanisms and identify emergent conservation in 15 of them

Abstract

Conservation laws are time-invariant properties that constrain many physical systems. For systems of chemical reactions, the law of mass conservation constrains how atoms flow between chemical species. Chemical reaction networks can display emergent conservation not explained by mass conservation: these hidden symmetries arise instead from coupled kinetics. Kinetic invariants emerge when branching reactions with proportional rates cause species concentrations to evolve in lockstep. We detect emergent conservation in a simplified atmospheric chemical mechanism of ozone formation through a data-driven analysis of simulated concentrations, a result matching the theoretical kinetic explanation. Surveying 35 widely used atmospheric chemical mechanisms spanning five orders of magnitude in complexity, we discover emergent conservation in 15 mechanisms. Kinetic invariants constrain the intrinsic dimensionality of chemical systems: mechanisms with emergent conservation evolve in lower-dimensional spaces than their size suggests. Identifying emergent conservation can provide theoretical bounds for exact mechanism reduction and uncover kinetic symmetries in atmospheric chemistry.

Plain Language Summary

Complex systems like the chemistry of the atmosphere have underlying symmetry and simplicity, where even under rapidly changing conditions, some things stay the same. One example of such a constant in time is the physical law of mass conservation, where matter cannot be created or destroyed, only rearranged in chemical reactions. However, mass conservation is not the only time-constant behavior in chemistry: we sometimes find emergent conservation that can't be explained by conservation of mass. Emergent conservation appears when certain reactions depend on the same chemical species, causing the rates of change of some species to always move in lockstep with each other. We can use this principle to reveal previously unknown dependencies and hidden relationships in atmospheric chemistry.

1 Introduction

The dynamic behavior of complex systems in the physical world is often constrained by time-invariant properties such as conservation laws. Conservation laws remain constant over time regardless of how quickly a dynamic system itself changes and are statements of fundamental symmetry and simplicity within complex systems. A canonical example is the law of mass conservation, attributed to the independent works of Mikhail Lomonosov and Antoine Lavoisier: matter is not created or destroyed in chemical reactions, only transformed as atoms are rearranged across chemical species (Lavoisier, 1789). In systems of chemical reactions, conservation of mass constrains the stoichiometry of reactions to preserve atom balances. In this work, we study an independent phenomenon: chemical systems representing atmospheric composition can display

emergent conservation distinct from the well-known law of mass conservation. This emergent conservation behavior arises from coupled kinetics within the system.

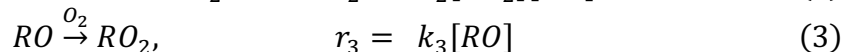
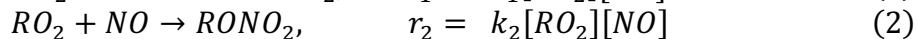
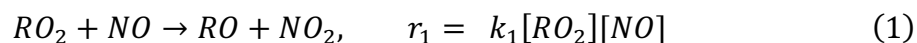
In the dynamical system that governs the chemical composition of the atmosphere, matter flows through a complex network of reactive chemical species whose behavior and time evolution are of societal and environmental importance. The coupled dynamics span many timescales of relevance, with highly reactive, short-lived species such as the hydroxyl radical, OH, determining the loss rates of pollutants (Levy, 1971) and long-lived greenhouse gases such as methane gas, CH₄, which has a chemical lifetime in the atmosphere of roughly a decade (Prather et al., 2012). Diurnal photochemical cycles and oxidative processes drive formation of secondary chemical species with adverse effects on air quality, such as the gas-phase respiratory irritant ozone (Leighton, 1961) and semi-volatile species which condense out of the gas phase to form particulate matter and atmospheric aerosol pollution (Donahue et al., 2006; Wexler & Seinfeld, 1991). These secondary pollutants are not directly emitted into the atmosphere but instead formed via a network of chemical reactions in the atmosphere. Elemental mass conservation in the form of stoichiometric atom balances constrains how chemical species are connected in these reaction networks, while reaction kinetics determine the time evolution of species as atoms flow between them. Numerical chemical mechanisms have been developed to represent these reaction networks, synthesizing fundamental first principles with empirical kinetic data from controlled laboratory experiments (Nguyen et al., 2023). These numerical mechanisms are used to predict and understand the behavior of the atmospheric chemical system under a wide variety of chemical regimes, environmental conditions, and possible future scenarios.

Concepts of invariance appear throughout the atmospheric chemistry literature, constraining the behavior of the complex system. The Leighton relationship relating ozone to nitrogen oxides under photostationary conditions is an example of a pseudo-steady state assumption (only approximately time-invariant) that identifies near-equilibrium behavior to obtain algebraic relationships between species (Leighton, 1961). Ozone isopleths, surfaces of constant ozone responses in chemical space, are an example of invariance in a different sense, and movement between isopleths reveals the nonlinear and non-monotonic dependencies of ozone production (Seinfeld & Pandis, 2016). Improved diagnostics for ozone production in chemical mechanisms have been built based on conservation of electron spin (Edwards & Evans, 2017). Each of these examples reveals where a complex nonlinear system is more constrained than it appears, yielding insight into nonlinear behavior and underlying simplicity. Elemental mass conservation, perhaps the most fundamental time-constant behavior, constrains how atoms flow between species and manifests as a set of stoichiometric invariants: linear combinations of species concentrations that are constant in time. These alone do not fully characterize the time-invariant behavior in the system. Here we show that atmospheric chemical mechanisms contain an independent class of invariants: emergent conservation arising not from stoichiometry but from coupled kinetics, where branching reactions create dependencies between the rates of change of different species (Blokhuys et al., 2025).

We identify emergent conservation in 15 out of 35 widely used atmospheric chemical mechanisms, revealing kinetic relationships that constrain their complexity.

2 Demonstration of emergent conservation in a three-reaction system

We first demonstrate the emergence of a kinetic invariant in a simple example of RO_2+NO branching reactions which are important in the photochemical production of ozone and secondary aerosol (Browne et al., 2013). Nitric oxide, NO, can be oxidized by a highly reactive peroxy radical RO_2 to form an alkoxy radical RO and NO_2 as products, propagating ozone-forming cycles. RO is also highly reactive and quickly further oxidizes to RO_2 in the Earth's oxygen-rich atmosphere. Alternatively, NO can react with RO_2 to instead form an organic nitrate species $RONO_2$. This second reaction channel occurs with a branching probability α_2 . This example 5-species, 3-reaction system is



where each reaction rate r_1, r_2, r_3 is proportional to the concentrations of each of its reactants via rate constant proportionalities k_1, k_2, k_3 : this kinetic formulation of reaction rates is known as the mass action law (Guldberg & Waage, 1879).

These reactions can also be represented by a 5-by-3 stoichiometric matrix on the left side of Figure 1, where columns represent the reactions and the entries represent stoichiometric coefficients (-1 or +1 for reactants or products, respectively). The stoichiometric matrix is a useful representation of a chemical system and has mathematical properties that correspond to some real-world properties of the system. Each reaction column is balanced with respect to nitrogen and the general "R" group (e.g. a hydrocarbon chain or an aromatic ring). This represents mass conservation for N and R assuming that this is a closed system (i.e., it is isolated from external sinks and sources within a time period of interest). Put differently, the total number of nitrogen atoms and number of R groups in the system is constant: this mass-conserving property can be

mathematically represented by 2 stoichiometric invariants shown in Figure 1, which are inherent properties of the stoichiometric matrix.

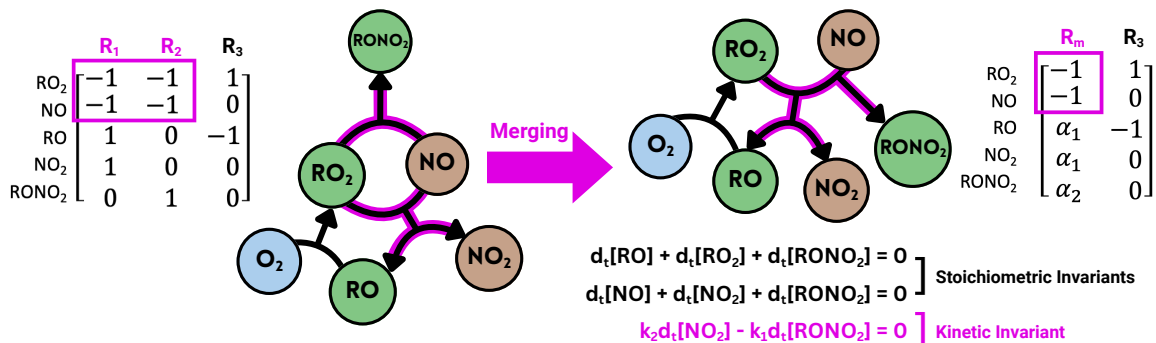


Figure 1. The law of mass action kinetics leads to proportional reaction rates for different product channels from the reaction of RO₂ and NO. In this simplified system of 5 species (rows) and 3 reactions (columns), coupled kinetics leads to only 2 effective reactions, shown in the merged matrix on the right hand side. There are 3 constraints on the system, the first 2 a consequence of mass conservation of N atoms and the R group respectively, and the third arising from emergent conservation. This emergent kinetic invariant links the rates of change of two species via rate constant proportionalities.

The stoichiometric matrix alone does not convey an additional invariant that emerges from coupled kinetics. As the law of mass action relates the rates of chemical reactions to their reactants, and the branching reactions 1 and 2 have the same co-reactants, these reactions proceed at proportional rates. NO₂ and RONO₂, as products of reactions 1 and 2 respectively, also have proportional time rates of change (denoted with d_t):

$$d_t[NO_2] = k_1[RO_2][NO] \quad (4)$$

$$d_t[RONO_2] = k_2[RO_2][NO] \quad (5)$$

Rearranging to solve for $[RO_2][NO]$ reveals a relation between the two rates of change:

$$\frac{d_t[NO_2]}{k_1} = [RO_2][NO] = \frac{d_t[RONO_2]}{k_2} \quad (6)$$

Rearranging once more, we identify an emergent *kinetic invariant*, a specific combination of rates that is always zero

$$k_2 d_t[NO_2] - k_1 d_t[RONO_2] = 0 \quad (7)$$

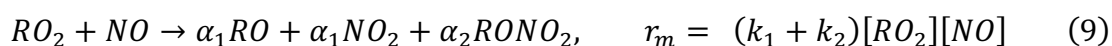
and integrating can show that a specific combination of species concentrations is always a constant in time:

$$k_2[NO_2] - k_1[RONO_2] = L \quad (8)$$

As with conservation of mass, this kinetic invariant appears in a closed system. As L is a function of two rate constants, the coefficients in the terms of L are only constant to the extent that the rate constants themselves are. The actual values of rate constants can

change as a result of changing environmental conditions (including temperature, pressure for termolecular reactions, and actinic flux for photolytic reactions). A kinetic invariant with specific values for the rate constants weighting the species in L could be theoretically identifiable in situations where environmental conditions are held constant but chemical conditions are still rapidly evolving, such as a chemistry operator step in a 3D atmospheric model, or in a controlled chamber experiment. Regardless of the values, a kinetic invariant emerges from this system that holds at any given instantaneous moment, revealing an additional relation of kinetic parameters and concentrations.

Proportional reaction rates linked by mass action kinetics reduce the effective number of reactions in a chemical system. Reactions 1 and 2 can be represented by a merged “effective reaction”



with an overall reaction rate r_m and stoichiometric weights $\alpha_1 = \frac{k_1}{k_1+k_2}$ and $\alpha_2 = 1 - \frac{k_1}{k_1+k_2} = \frac{k_2}{k_1+k_2}$ that are branching probabilities of the two reaction channels. The 5-by-2 merged matrix shown on the right side of Figure 1 accounts for coproduction: its reduced number of columns illustrates that the system has only two effective reactions. We define number of effective reactions as the number of columns in the merged matrix. Blokhuis et al. (2025) define the coproduction index γ as the number of reactions lost to merging, or the difference in number of reactions to number of effective reactions. This coproduction index γ can be calculated by the difference in number of columns of the stoichiometric matrix and the merged matrix, which for the RO+NO₂ example is 1.

We note that a lower number of effective reactions arising from coupled kinetics, or nonzero coproduction index, does not always imply emergent conservation. In some cases, the reduction of the reaction space from kinetic coproduction simply breaks a null cycle (Blokhuis et al., 2025). A null cycle is some combination of reactions that leaves the chemical state unchanged, with all species concentrations remaining constant. When branching reactions break a null cycle, they break redundancy in the reaction network rather than lead to a kinetic invariant. Section S1 demonstrates the breaking of a null cycle using the Chapman cycle as an example (Chapman, 1932).

In addition to revealing kinetic relationships that emerge from kinetic coupling in the reaction system, the presence of invariants constrains the dimensionality of this five-species system. Though the time evolution of all species can be written as a system of five coupled ordinary differential equations, seemingly five-dimensional, it actually evolves on a constrained two-dimensional manifold within that five-dimensional space, due to the presence of three invariants: two stoichiometric invariants and one emergent kinetic invariant. In section S2 we mathematically derive two ordinary differential equations that could be integrated to evolve two species concentrations forward in time with identical behavior to the full five equation system. In other words, using just the invariants, initial

concentrations of all species, and the two-equation system, the concentrations of all five species can be reconstructed at any point with perfect agreement to solve the five equation ODE system. More broadly, an improved understanding of constraints from emergent conservation complements the growing body of work on data-driven and machine learning models for reduced-order modeling of atmospheric composition, offering a theoretical framework to better motivate and understand the low-dimensional latent structures in atmospheric chemistry that such approaches utilize (Bodnar et al., 2025; Kelp et al., 2020; Liu et al., 2024; Wiser et al., 2023, 2025; Yang et al., 2024, 2025).

3 Agreement of data-driven discovery and theoretical basis for emergent conservation

We reconcile data-driven and theoretically grounded approaches for identifying emergent conservation using the Julia photochemical model (JPM), a simplified mechanism of ozone formation (Sturm & Silva, 2024; Sturm & Wexler, 2022). Because of its simplicity and highly constrained nature, JPM has been used to prototype methods for exploration of chemical mechanism behavior and data-driven emulation (Guo et al., 2024; Kircher & Votsmeier, 2025; Liu et al., 2024; Yang et al., 2024).

Emergent conservation was first discovered through a data-driven approach by Liu et al. (2024) using modeled concentration timeseries from JPM, before being subsequently related to mass action law kinetics by Blokhuis et al. (2025) who introduce this concept as the coproduction law in a theoretical framework for chemical reaction networks in general. In the present work, we use the updated version JPMv1.1 shown in Figure 2a. The updated JPMv1.1 is a 16-species, 13-reaction system that is highly constrained by design, conserving atoms of all four elements (C, N, H, and O) that make up the species composition (Sturm & Silva, 2024). Carbon is conserved both globally in the mechanism as well as locally in a subpool of carbon that flows from methylglyoxal and formaldehyde to carbon monoxide (yellow arrows in Figure 2a), distinct from the carbon that flows from methylglyoxal and acetaldehyde to the PAN cycle (this second conserved subpool can be obtained by a linear combination of global conservation and the first subpool). There are thus 5 stoichiometric invariants, all of which are a direct consequence of conservation of mass.

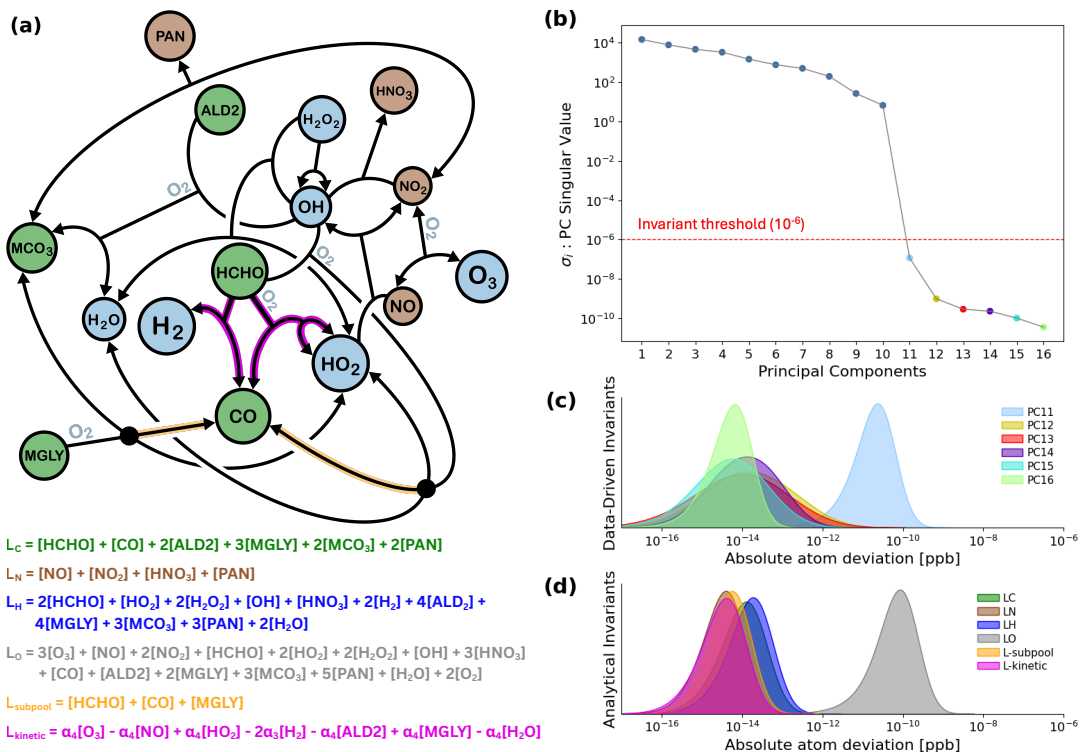


Figure 2. a) The Julia photochemical mechanism v1.1 and its invariants, visualized as a species hypergraph inspired by Blokhuis et al. (2025), b) vanishing singular values from principal component analysis on 50,000 simulated concentration timeseries from Sturm & Silva (2024), c) the extent of conservation of the corresponding eigenvectors of the vanishing principal components d) the extent of conservation of analytical invariants, for which the data-driven vanishing eigenvectors form a basis.

However, using a data-driven approach on concentration timeseries from JPM (Sturm & Silva, 2024), we detect six invariants – one extra invariant not explained by conservation of mass. More specifically, we apply principal component analysis (PCA) to the species concentrations to enumerate directions of minimum variance (Liu et al., 2024). Principal component directions of minimum variance are eigenvectors with singular values that vanish to zero, or in practice, fall below some threshold (Figure 2b). This approach itself is not new, and has been proposed for chemical systems as early as the 1960s, though with a focus on stoichiometric invariants (Aris & Mah, 1963) or identifying strongly interacting components for approximate mechanism reduction (Vajda et al., 1985). Our PCA analysis finds six linearly independent, vanishing principal component directions in the concentration timeseries. Each of these six eigenvectors represents a linear combination of species concentrations that is invariant over time regardless of how much species concentrations change. The distributions of numerical deviation from the invariants at all timesteps is shown in Figure 2c for each principal component direction, remaining under 10^{-9} ppb which is on the order of printing precision for the species with the highest concentrations in the timeseries.

Mass conservation can only explain five conserved properties in JPM. The sixth invariant discovered in the timeseries arises from the kinetics of the mechanism, where the

branching reactions of formaldehyde photolysis highlighted in magenta in Figure 2a can produce HO₂ to initiate a radical chain or instead produce the inert (as represented by this mechanism) species H₂. This kinetic redundancy reduces the number of reactions in JPM from 13 reactions to 12 effective reactions and leads to emergent conservation in the timeseries. Though more complex than RO₂+NO branching example, the kinetic invariant in JPM can still be derived analytically (section S3 in the Supplementary information). The six invariants in JPM are written as conserved combinations of species concentrations in Figure 2a, where α_3 and α_4 in the analytically derived kinetic invariant correspond to branching ratios.

The analytically derived kinetic invariant is perfectly conserved: it is as unchanging in the simulated timeseries as conservation of mass. Just like the vanishing eigenvectors from the data-driven approach in Figure 2c, the analytical expressions in Figure 2a are invariant to the limit of numerical precision: this invariance is shown in Figure 2d and remains within 10⁻¹¹ ppb except for the oxygen conservation law, which remains within 10⁻⁹ ppb due to printing precision limits. The data-driven and analytical invariant sets form a linear basis for each other, meaning that one is just a weighted combination of the other. As in the RO₂+NO example and section S2, the presence of six invariants in JPMv1.1 constrains the 16-species system to evolve with only 10 degrees of freedom. This provides an upper bound for the size of an even smaller reduced mechanism with identical behavior: a 10-species mechanism in combination with the six identified invariants could perfectly reconstruct the evolution of all 16 species in JPM at any point in time.

4 Survey of emergent conservation in atmospheric chemical mechanisms

We survey 35 atmospheric chemical mechanisms with varying complexity, scope, and configurations. Using edge lists of the species-reaction graph for each mechanism, we can construct the corresponding stoichiometric matrix and the merged matrix (see Figure 1 for example matrices of a simple system). From these matrices, we can use the linear algebra procedure in Appendix A to determine the number of stoichiometric invariants for each mechanism as well as whether emergent conservation arising from kinetic invariants will be found in the mechanism, assuming mass action kinetics for all reactions.

We discover emergent conservation in 15 of the 35 mechanisms. Mechanisms with emergent conservation are annotated with purple stars in Figure 3. Any mechanism with fewer effective reactions than species is *guaranteed* to have combinations of species concentrations that are invariant in time. Once mechanisms reach this 1:1 line from above, a further reduction in effective reaction space from branching reactions guarantees kinetic invariants. Four of the mechanisms with emergent conservation have a smaller number of effective reactions than species (the shaded area under the 1:1 line

in Figure 3): JPM v0.2 and v1.1, GEOS-Chem Hg (GC-Hg), and the Caltech Isoprene Mechanism (CIM).

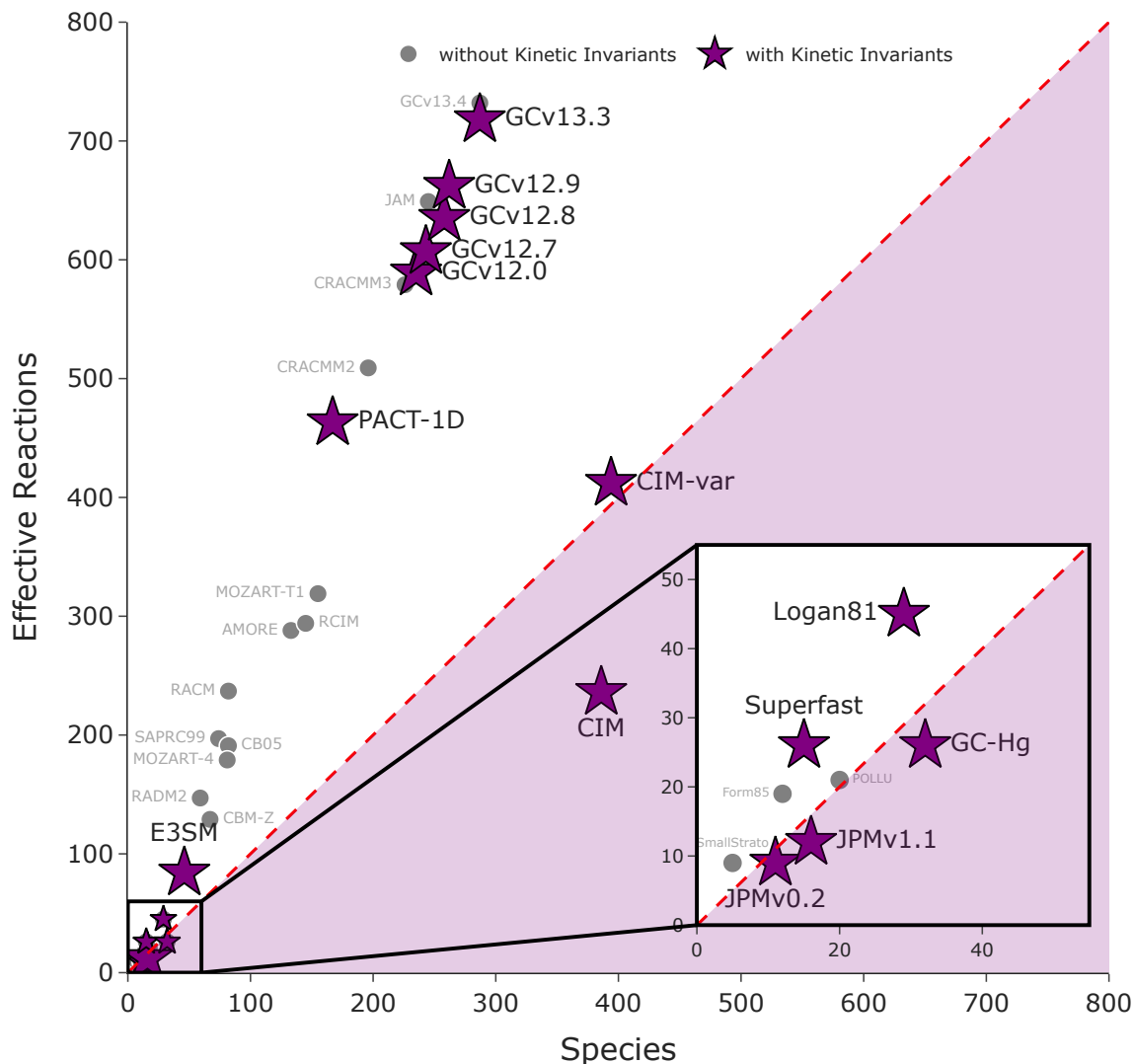


Figure 3. A summary of the emergent conservation survey in effective reactions vs species space, plotting 30 of the 35 mechanisms. Mechanisms with emergent conservation are denoted with purple stars. Due to scale constraints, GC14.6.3, CRI, MECCA, MCM, and MCM-PRAM are not shown but are present in Table S1 and in the log-scale Figure S2.

Emergent conservation can still arise in mechanisms above the 1:1 line of effective reactions to species. The Superfast and Logan81 mechanisms are small enough that it is possible to compute the symbolic cokernel of their merged matrices (see Appendix A) and

obtain an expression for their kinetic invariants. For Superfast, the single kinetic invariant is:

$$d_t[SO_2] + d_t[SO_4] + \left(\frac{k_{18} + 0.75k_{19}}{k_{18} + k_{19}}\right) d_t[DMS] = 0 \quad (10)$$

which corresponds to broken sulfur conservation. The Logan81 mechanism has a single kinetic invariant arising from N₂O branching reactions:

$$d_t[N_2O] + \left(\frac{k_6 + k_7}{k_6}\right) d_t[N_2] = 0 \quad (11)$$

A sensitivity test of holding N₂ concentration constant does not remove the presence of a kinetic invariant in Logan81, though it breaks one stoichiometric invariant corresponding to N conservation.

Emergent conservation can be found in versions of GEOS-Chem up to version 13.4. GEOS-Chem v12.0, v12.7, and v12.8 have 1 kinetic invariant. This number goes up to 2 kinetic invariants in GCv12.9 through v13.3. With the release of GCv13.4, where the update to chemistry included addition of heterogeneous sulfate and cloud processes, all emergent conservation disappears. Lack of emergent conservation has since persisted through the most recent version we surveyed, GCv14.6.3. Despite this, all versions of the GEOS-Chem mechanism have many proportional reactions and therefore have a high coproduction index γ , leading to a smaller number of effective reactions. For example, while the CRACMM3 mechanism has many fewer reactions than the mechanism used in GEOS-Chem v12.0, these mechanisms have nearly the same number of effective reactions (579 versus 591) due to the much higher coproduction index γ of GEOS-Chem.

The Caltech Isoprene Mechanism (CIM) has a very high coproduction index – 650 reactions with redundant coproducts correspond to 195 merged reactions for a total of 236 effective reactions between 386 species (placing CIM under the 1:1 line in Figure 3). This high amount of coproduction arises because in its default set up, CIM holds the concentrations of oxidants including HO_x, NO_x, and O₃ constant, assigning them to fixed species. The intended use case of the mechanism in its default configuration is not the overall impact of isoprene oxidation on these oxidant concentrations: rather it is used in this configuration to compare multiple isoprene oxidation mechanisms under identical oxidant conditions. However, a result of fixing oxidant conditions is that the intrinsic dimensionality of CIM is much smaller than its number of species (386) and reactions (886) might indicate – because of the large amount of emergent conservation, the 386-species CIM evolves with only 236 degrees of freedom. In other words, it would be possible to develop a zero-error reduced mechanism with 236 species based on CIM (61% the size) that could exactly reconstruct the full concentration timeseries of all 386 species in CIM. Though this hypothetical reduced mechanism would still be larger than the 133-species AMORE-Isoprene mechanism or the 145-species Reduced Plus Mechanism

(RCIM), it gives a theoretical upper bound for perfect mechanism reduction of CIM. This is an example of how emergent conservation can be used to obtain an upper limit for the size of reduced mechanisms.

As a sensitivity test of the effect of fixed oxidants on emergent conservation in the Caltech Isoprene Model, we switch all fixed oxidants to be variable species leaving only M, O₂, and two water tracers as fixed species. We call this 394-species configuration CIM-var, and find it has 412 effective reactions: in Figure 3, this puts it above the 1:1 line of effective reactions to species. Despite its location in Figure 3, a large number of emergent conservation properties – 17 kinetic invariants – still appear in CIM-var.

5 Discussion

The law of mass conservation is a well-known invariant property of chemical systems. However, atom conservation arising from reaction stoichiometry is not the only time-invariant behavior that can be detected in chemical mechanisms. We demonstrate that mass action kinetics in a chemical system with branching reactions can lead to emergent conservation in the form of kinetic invariants.

We reconcile two independent approaches for identifying conserved properties on a simplified mechanism of photochemical ozone formation: a data-driven approach that detects invariants in timeseries using principal component analysis, and a first-principles approach using stoichiometric mass balances and the law of mass action kinetics. We find agreement between these two approaches, each identifying six invariants in the Julia Photochemical Mechanism, one of which is an emergent kinetic invariant. The first principles approach can be generalized to work for any general chemical mechanism with mass action kinetics (Blokhuis et al., 2025), which we then apply to a survey of 35 commonly used atmospheric chemical mechanisms.

Emergent conservation is not just a property of simplified chemical mechanisms. We discover emergent conservation in 15 out of 35 mechanisms, including the Caltech Isoprene Mechanism CIM (Wennberg et al., 2018). CIM is one of the more complex mechanisms surveyed and has the largest number of kinetic invariants. Emergent conservation properties in CIM constrain its dimensionality, meaning the chemical system evolves on an exact manifold constrained by emergent conservation. This provides an upper bound for the size of a reduced isoprene mechanism that with a fraction of the species (~61%) could perfectly replicate the behavior of CIM.

This analysis was limited to numerical chemical mechanisms. While kinetic invariants are unlikely to be purely numerical artifacts – if a chemical mechanism with emergent conservation contains sufficiently representative reactions of real-world or laboratory-obtainable chemical conditions, it should be theoretically possible to detect – kinetic invariants have yet to be observed in measurements. Challenges in detecting emergent

conservation in chamber experiments could arise from measurement noise, wall loss or dilution loss that violate closed system assumptions, or perturbations in environmental conditions that would change the values of rate constants in the kinetic invariant expressions. On the other hand, chamber experiments are a promising setting in which to study emergent conservation, as often small numbers of precursors are studied in highly controlled chemical and environmental conditions to obtain rate constants and other kinetic parameters, such as estimation of branching ratios in different branching reaction channels (e.g. Barber et al., 2024; Murphy et al., 2023). For example, the *n*-pentyl nitrite photolysis experiments in Barber et al. (2024) contain sufficient branching reactions that emergent conservation, if detectable, could be used to constrain the time evolution of the system to one single direction from which rate constants and branching ratios could be obtained.

Beyond its theoretical implications for mechanism reduction, the detection of emergent conservation in controlled chamber experiments could be used to constrain branching ratios and reaction kinetics, where a fundamental symmetry of chemical systems could be leveraged as a complementary theoretical framework to enhance experimental design and interpretation. By revealing hidden structure in chemical mechanisms, identifying emergent conservation can provide new pathways for bounding mechanism complexity, constraining kinetic parameters, and uncovering previously unknown symmetries in atmospheric oxidation chemistry.

Appendix A: General method for identifying emergent conservation from kinetics

While the emergence of a kinetic invariant may seem immediately intuitive for a simple illustrative example like the 3-reaction system of RO_2+NO branching ratios, larger systems can have more complex or more deeply hidden emergent conservation. This section briefly outlines the linear algebra for a general procedure to detect emergent kinetic invariants.

We obtain the number of stoichiometric invariants from conservation of mass by calculating the dimension of the cokernel (left null space) of the stoichiometric matrix of a chemical mechanism, such as the matrix on the left side of Figure 1. To account for kinetic coupling, we merge reactions with duplicate co-reactant sets and therefore proportional rates, using rate constants to proportionally weight each reaction in the merge. To find the total number of invariants, we then recompute the dimensionality of the cokernel of the merged matrix (such as the matrix on the right side of Figure 1) – symbolically for small mechanisms and numerically for larger mechanisms (further details in section S4). As the merging operations preserve mass balances and all stoichiometric invariants, any resulting addition to the dimension of the cokernel of the merged matrix is a result of emergent conservation arising from kinetic invariants.

Appendix B: A graph library of atmospheric chemical mechanisms

As part of this work, we publish a graph library of oxidative atmospheric mechanisms, available at <https://doi.org/10.5281/zenodo.19928697> (Sturm et al., 2026). This library contains edge lists of 35 chemical mechanisms in the species-reaction graph format (Feinberg, 2019; Silva et al., 2021). We then apply the generalized linear algebra approach of detecting emergent conservation to all mechanisms. As many mechanisms are written using the Kinetic PreProcessor KPP (Damian et al., 2002; Lin et al., 2023) we formalize the modifications made to KPP to create the species-reaction edge list for the GEOS-Chem mechanism in prior work (Getter et al., 2025; Li et al., 2025). These updates to the KPP codebase are released as part of KPP 3.4.0 with the option to automatically generate the edge list of the species-reaction graph for any chemical mechanism. For all mechanisms, we assume mass action kinetics when performing the merging operations and linear algebra described in Appendix A. However, we do note that exceptions to this could be made: a reaction in KPP can be assigned to be a constant rate (not a function of reactant concentrations) or be a function of an oxidant pool such as an RO₂ summation from many peroxy radical species in the system not listed as explicit reactants in the reaction (as in the MCM).

The following two paragraphs introduce each of the 35 mechanisms included in the survey, which span orders of magnitude in complexity and serve varying use cases. At the most simplified end, we include a set of 8 representative chemistry mechanisms (each containing under 100 reactions) that have parameterized, incomplete chemistry and/or limited scope representing a narrow set of species. This low complexity set includes the KPP demonstration mechanism of simplified stratospheric chemistry Small Strato (Damian et al., 2002), the Julia Photochemical Model JPM v0.2 (Sturm & Wexler, 2022) and JPM v1.1 (Sturm & Silva, 2024), the Superfast Chemistry mechanism (Brown-Steiner et al., 2018; Cameron-Smith et al., 2006) obtained in KPP format from Kelp et al. (2022), a formaldehyde oxidation mechanism Form85 (Vajda et al., 1985), a simplified nitrogen and sulfur pollution mechanism POLLU (Verwer, 1994), the GEOS-Chem Hg mechanism used to simulate mercury oxidation and transport (Shah et al., 2021), and the gas-phase mechanism of an early description of tropospheric chemistry resembling the state of the science at that time (Logan et al., 1981), hereafter referred to as Logan81. On the other side of the complexity spectrum, we include the edge list of the near-explicit chemical mechanism MCM v3.3.1, with 5,832 species interacting via 16,698 reactions in a much more complete representation of atmospheric chemistry (Bloss et al., 2005; Jenkin et al., 1997, 2012, 2015; Saunders et al., 2003). We further extend this version of MCM with the Peroxy Radical Autooxidation Mechanism PRAM (Roldin, 2019; Roldin et al., 2019). The coupled pair of mechanisms MCM-PRAM has 6,041 species interacting in 18,478 reactions.

In between these extreme ends of simplification and near-explicit representation span a group of 25 chemical mechanisms with moderate complexity (roughly 40-800 species and 100-2300 reactions). The design goal of these moderate-complexity mechanisms is either

to broadly capture many atmospherically relevant chemical regimes while remaining small enough to fit in the grid cells of a 3D chemical transport model or provide detailed focus on a certain set of reactive species such as halogens or oxidation of biogenic volatile organic compounds. In this moderate complexity group, we include E3SM-chem used in 3D climate modeling (Tang et al., 2025), the carbon bond mechanism CBM-Z (Zaveri & Peters, 1999), the regional acid deposition model RADM2 (Stockwell et al., 1990), SAPRC-99 (Carter, 2000), and the carbon bond mechanism CB05-TUCL updated with toluene reactions (Whitten et al., 2010) and a chlorine extension (Tanaka et al., 2003). We include two versions of the Model for Ozone and Related chemical Tracers, MOZART-4 (Emmons et al., 2010) and MOZART-T1 (Emmons et al., 2020). We include the Regional Atmospheric Chemistry Mechanism RACM (Stockwell et al., 1997) which is a predecessor to two included versions of the Community Regional Atmospheric Multiphase Mechanism CRACMM2 and CRACMM3 (Pye et al., 2023; Skipper et al., 2024). Also within the RACM family, we include the PACT-1D-HALOGENSv1.1 mechanism (Ahmed et al., 2022) which is based on RACM2 (Goliff et al., 2013) with extensions for halogen chemistry. We also compare 7 versions of GEOS-Chem (Bey et al., 2001) from v12.0.0 to v14.6.3, spanning major model updates. We include 4 mechanisms with a focus on isoprene oxidation: these are the Caltech isoprene mechanism CIM (Bates & Wennberg, 2017; Wennberg et al., 2018), a configuration of CIM with variable oxidants rather than the default fixed-oxidant approach which we call CIM-var, a manually reduced mechanism Caltech Reduced Plus RCIMv5, and an algorithmically reduced mechanism AMORE-Isoprene 2.0 with 133 species and 330 reactions, created using an automated graph theoretical approach to reduce an initially extended version of CIM (Wiser et al., 2025). We include two mechanisms from the CAABA/MECCA codebase (Sander, 2024; Sander et al., 2019): MECCAv4.6.0 and the Jülich Atmospheric Mechanism JAMv2.0 (Schultz et al., 2018). Finally we include the Chemical Reactive Intermediates mechanism CRI v2.2 (Jenkin et al., 2008, 2019; Watson et al., 2008). Table S1 contains a comprehensive overview of all mechanisms, including their relevant reference sources and notes, as well as the results of the survey: amount of coproduction, number of stoichiometric invariants, and number of emergent kinetic invariants.

Acknowledgments

This work was supported by NSF Grant AGS-2228923, NSF Grant AGS-2441535, and NASA Grant 80NSSC23K0523. Obin Sturm acknowledges funding from the Diane Sonosky Montgomery and Jerol Sonosky Graduate Fellowship for Environmental Sustainability Research. We thank Bob Yantosca and Rolf Sander for reviewing and supporting the updates to the Kinetic PreProcessor.

Data Availability Statement

All scripts and data used in the analysis are available at 10.5281/zenodo.19928145 (Rodriguez & Sturm, 2026). The graph library of oxidative atmospheric mechanisms is available at 10.5281/zenodo.19928697 (Sturm et al., 2026).

Conflict of Interest Disclosure

The authors declare there are no conflicts of interest for this manuscript.

References

- Ahmed, S., Thomas, J. L., Tuite, K., Stutz, J., Flocke, F., Orlando, J. J., et al. (2022). The Role of Snow in Controlling Halogen Chemistry and Boundary Layer Oxidation During Arctic Spring: A 1D Modeling Case Study. *Journal of Geophysical Research: Atmospheres*, 127(5), e2021JD036140. <https://doi.org/10.1029/2021JD036140>
- Aris, R., & Mah, R. H. S. (1963). Independence of Chemical Reactions. *Industrial & Engineering Chemistry Fundamentals*, 2(2), 90–94. <https://doi.org/10.1021/i160006a002>
- Barber, V. P., LeMar, L. N., Li, Y., Zheng, J. W., Keutsch, F. N., & Kroll, J. H. (2024). Enhanced Organic Nitrate Formation from Peroxy Radicals in the Condensed Phase. *Environmental Science & Technology Letters*, 11(9), 975–980. <https://doi.org/10.1021/acs.estlett.4c00473>
- Bates, K., & Wennberg, P. (2017). Isoprene Oxidation Model. Retrieved from <https://data.caltech.edu/records/x88rk-wca37>
- Bey, I., Jacob, D. J., Yantosca, R. M., Logan, J. A., Field, B. D., Fiore, A. M., et al. (2001). Global modeling of tropospheric chemistry with assimilated meteorology: Model description and evaluation. *Journal of Geophysical Research: Atmospheres*, 106(D19), 23073–23095. <https://doi.org/10.1029/2001JD000807>
- Blokhuis, A., Kuppeveld, M. van, Weem, D. van de, & Pollice, R. (2025, June 15). On data and dimension in chemistry -- irreversibility, concealment and emergent conservation laws. arXiv. <https://doi.org/10.48550/arXiv.2306.09553>
- Bloss, C., Wagner, V., Jenkin, M. E., Volkamer, R., Bloss, W. J., Lee, J. D., et al. (2005). Development of a detailed chemical mechanism (MCMv3.1) for the atmospheric oxidation of aromatic hydrocarbons. *Atmospheric Chemistry and Physics*, 5(3), 641–664. <https://doi.org/10.5194/acp-5-641-2005>
- Bodnar, C., Bruinsma, W. P., Lucic, A., Stanley, M., Allen, A., Brandstetter, J., et al. (2025). A foundation model for the Earth system. *Nature*, 641(8065), 1180–1187. <https://doi.org/10.1038/s41586-025-09005-y>
- Browne, E. C., Min, K.-E., Wooldridge, P. J., Apel, E., Blake, D. R., Brune, W. H., et al. (2013). Observations of total RONO₂ over the boreal forest: NO_x sinks and HNO₃ sources. *Atmospheric Chemistry and Physics*, 13(9), 4543–4562. <https://doi.org/10.5194/acp-13-4543-2013>
- Brown-Steiner, B., Selin, N. E., Prinn, R., Tilmes, S., Emmons, L., Lamarque, J.-F., & Cameron-Smith, P. (2018). Evaluating simplified chemical mechanisms within present-day simulations of the Community Earth System Model version 1.2 with CAM4 (CESM1.2 CAM-chem): MOZART-4 vs. Reduced Hydrocarbon vs. Super-Fast chemistry. *Geoscientific Model Development*, 11(10), 4155–4174. <https://doi.org/10.5194/gmd-11-4155-2018>
- Cameron-Smith, P., Lamarque, J.-F., Connell, P., Chuang, C., & Vitt, F. (2006). Toward an Earth system model: atmospheric chemistry, coupling, and petascale computing. *Journal of Physics: Conference Series*, 46(1), 343. <https://doi.org/10.1088/1742-6596/46/1/048>
- Carter, W. P. L. (2000). Documentation for the SAPRC-99 Chemical Mechanism And Updated VOC Reactivity Scales. Retrieved February 12, 2026, from <https://intra.engr.ucr.edu/~carter/reactdat.htm>
- Chapman, S. (1932). Discussion of memoirs. On a theory of upper-atmospheric ozone. *Quarterly Journal of the Royal Meteorological Society*, 58(243), 11–13. <https://doi.org/10.1002/qj.49705824304>

- Damian, V., Sandu, A., Damian, M., Potra, F., & Carmichael, G. R. (2002). The kinetic preprocessor KPP—a software environment for solving chemical kinetics. *Computers & Chemical Engineering*, *26*(11), 1567–1579. [https://doi.org/10.1016/S0098-1354\(02\)00128-X](https://doi.org/10.1016/S0098-1354(02)00128-X)
- Donahue, N. M., Robinson, A. L., Stanier, C. O., & Pandis, S. N. (2006). Coupled Partitioning, Dilution, and Chemical Aging of Semivolatile Organics. *Environmental Science & Technology*, *40*(8), 2635–2643. <https://doi.org/10.1021/es052297c>
- Edwards, P. M., & Evans, M. J. (2017). A new diagnostic for tropospheric ozone production. *Atmospheric Chemistry and Physics*, *17*(22), 13669–13680. <https://doi.org/10.5194/acp-17-13669-2017>
- Emmons, L. K., Schwantes, R. H., Orlando, J. J., Tyndall, G., Kinnison, D., Lamarque, J.-F., et al. (2020). The Chemistry Mechanism in the Community Earth System Model Version 2 (CESM2). *Journal of Advances in Modeling Earth Systems*, *12*(4), e2019MS001882. <https://doi.org/10.1029/2019MS001882>
- Emmons, Louisa. K., Walters, S., Hess, P. G., Lamarque, J.-F., Pfister, G. G., Fillmore, D., et al. (2010). Description and evaluation of the Model for Ozone and Related chemical Tracers, version 4 (MOZART-4). *Geoscientific Model Development*, *3*(1), 43–67. <https://doi.org/10.5194/gmd-3-43-2010>
- Feinberg, M. (2019). The Species-Reaction Graph. In M. Feinberg (Ed.), *Foundations of Chemical Reaction Network Theory* (pp. 205–240). Cham: Springer International Publishing. https://doi.org/10.1007/978-3-030-03858-8_11
- Getter, D., Sturm, P. O., & Silva, S. J. (2025). Data-Driven Discovery of Atmospheric Chemical Reactions. *Journal of Geophysical Research: Machine Learning and Computation*, *2*(4), e2025JH000895. <https://doi.org/10.1029/2025JH000895>
- Goliff, W. S., Stockwell, W. R., & Lawson, C. V. (2013). The regional atmospheric chemistry mechanism, version 2. *Atmospheric Environment*, *68*, 174–185. <https://doi.org/10.1016/j.atmosenv.2012.11.038>
- Guldberg, C. M., & Waage, P. (1879). Ueber die chemische Affinität. § 1. Einleitung. *Journal Für Praktische Chemie*, *19*(1), 69–114. <https://doi.org/10.1002/prac.18790190111>
- Guo, L., Yang, X., Zheng, Z., Riemer, N., & Tessum, C. W. (2024, July 12). Uncertainty Quantification in Reduced-Order Gas-Phase Atmospheric Chemistry Modeling using Ensemble SINDy. arXiv. <https://doi.org/10.48550/arXiv.2407.09757>
- Jenkin, M. E., Saunders, S. M., & Pilling, M. J. (1997). The tropospheric degradation of volatile organic compounds: a protocol for mechanism development. *Atmospheric Environment*, *31*(1), 81–104. [https://doi.org/10.1016/S1352-2310\(96\)00105-7](https://doi.org/10.1016/S1352-2310(96)00105-7)
- Jenkin, M. E., Watson, L. A., Utembe, S. R., & Shallcross, D. E. (2008). A Common Representative Intermediates (CRI) mechanism for VOC degradation. Part 1: Gas phase mechanism development. *Atmospheric Environment*, *42*(31), 7185–7195. <https://doi.org/10.1016/j.atmosenv.2008.07.028>
- Jenkin, M. E., Wyche, K. P., Evans, C. J., Carr, T., Monks, P. S., Alfarra, M. R., et al. (2012). Development and chamber evaluation of the MCM v3.2 degradation scheme for β -caryophyllene. *Atmospheric Chemistry and Physics*, *12*(11), 5275–5308. <https://doi.org/10.5194/acp-12-5275-2012>
- Jenkin, M. E., Young, J. C., & Rickard, A. R. (2015). The MCM v3.3.1 degradation scheme for isoprene. *Atmospheric Chemistry and Physics*, *15*(20), 11433–11459. <https://doi.org/10.5194/acp-15-11433-2015>
- Jenkin, M. E., Khan, M. A. H., Shallcross, D. E., Bergström, R., Simpson, D., Murphy, K. L. C., & Rickard, A. R. (2019). The CRI v2.2 reduced degradation scheme for isoprene. *Atmospheric Environment*, *212*, 172–182. <https://doi.org/10.1016/j.atmosenv.2019.05.055>
- Kelp, M. M., Jacob, D. J., Kutz, J. N., Marshall, J. D., & Tessum, C. W. (2020). Toward Stable, General Machine-Learned Models of the Atmospheric Chemical System. *Journal of Geophysical Research: Atmospheres*, *125*(23), e2020JD032759. <https://doi.org/10.1029/2020JD032759>
- Kelp, M. M., Jacob, D. J., Lin, H., & Sulprizio, M. P. (2022). An Online-Learned Neural Network Chemical Solver for Stable Long-Term Global Simulations of Atmospheric Chemistry. *Journal of Advances in Modeling Earth Systems*, *14*(6), e2021MS002926. <https://doi.org/10.1029/2021MS002926>
- Kircher, T., & Votsmeier, M. (2025). Machine Learning Surrogate Models for Mechanistic Kinetics: Embedding Atom Balance and Positivity. *The Journal of Physical Chemistry Letters*, *16*(19), 4715–4723. <https://doi.org/10.1021/acs.jpcclett.5c00602>
- Lavoisier, A. L. (1789). *Traité élémentaire de chimie : présenté dans un ordre nouveau et d'après les découvertes modernes ; avec figures*. A Paris, Chez Cuchet, libraire, rue et Hôtel Serpente. Retrieved from <http://archive.org/details/traitlementairede01lavo>
- Leighton, P. A. (1961). *Photochemistry of Air Pollution*. Academic Press.
- Levy, H. (1971). Normal Atmosphere: Large Radical and Formaldehyde Concentrations Predicted. *Science*, *173*(3992), 141–143. <https://doi.org/10.1126/science.173.3992.141>

- Li, E. W., Sturm, P. O., Silva, S. J., Barber, V. A., & Keller, C. A. (2025). Characterizing the Speed of Chemical Cycling in the Atmosphere. *Geophysical Research Letters*, *52*(4), e2024GL111021. <https://doi.org/10.1029/2024GL111021>
- Lin, H., Long, M. S., Sander, R., Sandu, A., Yantosca, R. M., Estrada, L. A., et al. (2023). An Adaptive Auto-Reduction Solver for Speeding Up Integration of Chemical Kinetics in Atmospheric Chemistry Models: Implementation and Evaluation in the Kinetic Pre-Processor (KPP) Version 3.0.0. *Journal of Advances in Modeling Earth Systems*, *15*(2), e2022MS003293. <https://doi.org/10.1029/2022MS003293>
- Liu, Z., Sturm, P. O., Bharadwaj, S., Silva, S. J., & Tegmark, M. (2024). Interpretable conservation laws as sparse invariants. *Physical Review E*, *109*(2), L023301. <https://doi.org/10.1103/PhysRevE.109.L023301>
- Logan, J. A., Prather, M. J., Wofsy, S. C., & McElroy, M. B. (1981). Tropospheric chemistry: A global perspective. *Journal of Geophysical Research: Oceans*, *86*(C8), 7210–7254. <https://doi.org/10.1029/JC086iC08p07210>
- Murphy, S. E., Crounse, J. D., Møller, K. H., Rezugui, S. P., Hafeman, N. J., Park, J., et al. (2023). Accretion product formation in the self-reaction of ethene-derived hydroxy peroxy radicals. *Environmental Science: Atmospheres*, *3*(5), 882–893. <https://doi.org/10.1039/D3EA00020F>
- Nguyen, T. B., Bates, K. H., Buenconsejo, R. S., Charan, S. M., Cavanna, E. E., Cocker, D. R. I., et al. (2023). Overview of ICARUS—A Curated, Open Access, Online Repository for Atmospheric Simulation Chamber Data. *ACS Earth and Space Chemistry*. <https://doi.org/10.1021/acsearthspacechem.3c00043>
- Prather, M. J., Holmes, C. D., & Hsu, J. (2012). Reactive greenhouse gas scenarios: Systematic exploration of uncertainties and the role of atmospheric chemistry. *Geophysical Research Letters*, *39*(9). <https://doi.org/10.1029/2012GL051440>
- Pye, H. O. T., Place, B. K., Murphy, B. N., Seltzer, K. M., D'Ambro, E. L., Allen, C., et al. (2023). Linking gas, particulate, and toxic endpoints to air emissions in the Community Regional Atmospheric Chemistry Multiphase Mechanism (CRACMM). *Atmospheric Chemistry and Physics*, *23*(9), 5043–5099. <https://doi.org/10.5194/acp-23-5043-2023>
- Rodriguez, B. L. G., & Sturm, P. O. (2026, April 30). Code and Data for Rodriguez et al., Emergent conservation in atmospheric chemical mechanisms. Zenodo. <https://doi.org/10.5281/zenodo.19928145>
- Roldin, P. (2019). Peroxy Radical Autoxidation Mechanism (PRAM) [Data set]. *Supplement to: Roldin, Pontus; Ehn, Mikael; Kurtén, Theo; Olenius, Tinja; Rissanen, Matti P; Sarnela, Nina; Elm, Jonas; Rantala, Pekka; Hao, Liqing; Hyttinen, Noora; Heikkinen, Liine; Worsnop, Douglas R; Pichelstorfer, Lukas; Xavier, Carlton; Clusius, Petri; Öström, Emilie; Petäjä, Tuukka; Kulmala, Markku; Vehkamäki, Hanna; Virtanen, Annele; Riipinen, Ilona; Boy, Michael (2019): The role of highly oxygenated organic molecules in the Boreal aerosol-cloud-climate system. Nature Communications*, *10*(1), <https://doi.org/10.1038/s41467-019-12338-8>. PANGAEA. <https://doi.org/10.1594/PANGAEA.905102>
- Roldin, P., Ehn, M., Kurtén, T., Olenius, T., Rissanen, M. P., Sarnela, N., et al. (2019). The role of highly oxygenated organic molecules in the Boreal aerosol-cloud-climate system. *Nature Communications*, *10*(1), 4370. <https://doi.org/10.1038/s41467-019-12338-8>
- Sander, R. (2024). MEXPLORER 1.0.0 – a mechanism explorer for analysis and visualization of chemical reaction pathways based on graph theory. *Geoscientific Model Development*, *17*(6), 2419–2425. <https://doi.org/10.5194/gmd-17-2419-2024>
- Sander, R., Baumgaertner, A., Cabrera-Perez, D., Frank, F., Gromov, S., Grooß, J.-U., et al. (2019). The community atmospheric chemistry box model CAABA/MECCA-4.0. *Geoscientific Model Development*, *12*(4), 1365–1385. <https://doi.org/10.5194/gmd-12-1365-2019>
- Saunders, S. M., Jenkin, M. E., Derwent, R. G., & Pilling, M. J. (2003). Protocol for the development of the Master Chemical Mechanism, MCM v3 (Part A): tropospheric degradation of non-aromatic volatile organic compounds. *Atmospheric Chemistry and Physics*, *3*(1), 161–180. <https://doi.org/10.5194/acp-3-161-2003>
- Schultz, M. G., Stadler, S., Schröder, S., Taraborrelli, D., Franco, B., Krefting, J., et al. (2018). The chemistry–climate model ECHAM6.3-HAM2.3-MOZ1.0. *Geoscientific Model Development*, *11*(5), 1695–1723. <https://doi.org/10.5194/gmd-11-1695-2018>
- Seinfeld, J. H., & Pandis, S. N. (2016). *Atmospheric Chemistry and Physics: From Air Pollution to Climate Change*. John Wiley & Sons.
- Shah, V., Jacob, D. J., Thackray, C. P., Wang, X., Sunderland, E. M., Dibble, T. S., et al. (2021). Improved Mechanistic Model of the Atmospheric Redox Chemistry of Mercury. *Environmental Science & Technology*, *55*(21), 14445–14456. <https://doi.org/10.1021/acs.est.1c03160>
- Silva, S. J., Burrows, S. M., Evans, M. J., & Halappanavar, M. (2021). A Graph Theoretical Intercomparison of Atmospheric Chemical Mechanisms. *Geophysical Research Letters*, *48*(1), e2020GL090481. <https://doi.org/10.1029/2020GL090481>
- Skipper, T. N., D'Ambro, E. L., Wisner, F. C., McNeill, V. F., Schwantes, R. H., Henderson, B. H., et al. (2024). Role of chemical production and depositional losses on formaldehyde in the Community Regional Atmospheric

- Chemistry Multiphase Mechanism (CRACMM). *Atmospheric Chemistry and Physics*, 24(22), 12903–12924. <https://doi.org/10.5194/acp-24-12903-2024>
- Stockwell, W. R., Middleton, P., Chang, J. S., & Tang, X. (1990). The second generation regional acid deposition model chemical mechanism for regional air quality modeling. *Journal of Geophysical Research: Atmospheres*, 95(D10), 16343–16367. <https://doi.org/10.1029/JD095iD10p16343>
- Stockwell, W. R., Kirchner, F., Kuhn, M., & Seefeld, S. (1997). A new mechanism for regional atmospheric chemistry modeling. *Journal of Geophysical Research: Atmospheres*, 102(D22), 25847–25879. <https://doi.org/10.1029/97JD00849>
- Sturm, P. O., & Silva, S. J. (2024). A Nudge to the Truth: Atom Conservation as a Hard Constraint in Models of Atmospheric Composition Using a Species-Weighted Correction. *ACS ES&T Air*. <https://doi.org/10.1021/acsestair.4c00220>
- Sturm, P. O., & Wexler, A. S. (2022). Conservation laws in a neural network architecture: enforcing the atom balance of a Julia-based photochemical model (v0.2.0). *Geoscientific Model Development*, 15(8), 3417–3431. <https://doi.org/10.5194/gmd-15-3417-2022>
- Sturm, P. O., Rodriguez, B. L. G., Getter, D., & Silva, S. J. (2026). Graph Library of Oxidative Atmospheric Mechanisms [Data set]. Zenodo. <https://doi.org/10.5281/zenodo.19928697>
- Tanaka, P. L., Allen, D. T., McDonald-Buller, E. C., Chang, S., Kimura, Y., Mullins, C. B., et al. (2003). Development of a chlorine mechanism for use in the carbon bond IV chemistry model. *Journal of Geophysical Research: Atmospheres*, 108(D4). <https://doi.org/10.1029/2002JD002432>
- Tang, Q., Prather, M. J., Ke, Z., Xie, J., Lee, H.-H., Wu, M., et al. (2025). Interactive Gas Chemistry for Enhanced Science Capabilities of the Energy Exascale Earth System Model Version 3. *Journal of Advances in Modeling Earth Systems*, 17(10), e2025MS005062. <https://doi.org/10.1029/2025MS005062>
- Vajda, S., Valko, P., & Turányi, T. (1985). Principal component analysis of kinetic models. *International Journal of Chemical Kinetics*, 17(1), 55–81. <https://doi.org/10.1002/kin.550170107>
- Verwer, J. G. (1994). Gauss–Seidel Iteration for Stiff ODEs from Chemical Kinetics. *SIAM Journal on Scientific Computing*, 15(5), 1243–1250. <https://doi.org/10.1137/0915076>
- Watson, L. A., Shallcross, D. E., Utembe, S. R., & Jenkin, M. E. (2008). A Common Representative Intermediates (CRI) mechanism for VOC degradation. Part 2: Gas phase mechanism reduction. *Atmospheric Environment*, 42(31), 7196–7204. <https://doi.org/10.1016/j.atmosenv.2008.07.034>
- Wennberg, P. O., Bates, K. H., Crouse, J. D., Dodson, L. G., McVay, R. C., Mertens, L. A., et al. (2018). Gas-Phase Reactions of Isoprene and Its Major Oxidation Products. *Chemical Reviews*, 118(7), 3337–3390. <https://doi.org/10.1021/acs.chemrev.7b00439>
- Wexler, A. S., & Seinfeld, J. H. (1991). Second-generation inorganic aerosol model. *Atmospheric Environment. Part A. General Topics*, 25(12), 2731–2748. [https://doi.org/10.1016/0960-1686\(91\)90203-J](https://doi.org/10.1016/0960-1686(91)90203-J)
- Whitten, G. Z., Heo, G., Kimura, Y., McDonald-Buller, E., Allen, D. T., Carter, W. P. L., & Yarwood, G. (2010). A new condensed toluene mechanism for Carbon Bond: CB05-TU. *Atmospheric Environment*, 44(40), 5346–5355. <https://doi.org/10.1016/j.atmosenv.2009.12.029>
- Wiser, F., Place, B. K., Sen, S., Pye, H. O. T., Yang, B., Westervelt, D. M., et al. (2023). AMORE-Isoprene v1.0: a new reduced mechanism for gas-phase isoprene oxidation. *Geoscientific Model Development*, 16(6), 1801–1821. <https://doi.org/10.5194/gmd-16-1801-2023>
- Wiser, F., Sen, S., Wang, Z., Lee-Taylor, J., Barsanti, K. C., Orlando, J., et al. (2025). A graph theory-based algorithm for the reduction of atmospheric chemical mechanisms. *PNAS Nexus*, 4(9), pgaf273. <https://doi.org/10.1093/pnasnexus/pgaf273>
- Yang, X., Guo, L., Zheng, Z., Riemer, N., & Tessum, C. W. (2024). Atmospheric Chemistry Surrogate Modeling With Sparse Identification of Nonlinear Dynamics. *Journal of Geophysical Research: Machine Learning and Computation*, 1(2), e2024JH000132. <https://doi.org/10.1029/2024JH000132>
- Yang, X., Guo, L., & Tessum, C. W. (2025). Atmospheric Chemistry Surrogate Modeling With Sparse Identification of Mass Action Dynamics. *Journal of Geophysical Research: Machine Learning and Computation*, 2(4), e2025JH000731. <https://doi.org/10.1029/2025JH000731>
- Zaveri, R. A., & Peters, L. K. (1999). A new lumped structure photochemical mechanism for large-scale applications. *Journal of Geophysical Research: Atmospheres*, 104(D23), 30387–30415. <https://doi.org/10.1029/1999JD900876>

Supporting Information

Text S1. Demonstration of a broken null cycle in the Chapman mechanism

Branching reactions do not always produce an emergent invariant like in the $RO_2 + NO$ example. In this section we demonstrate how this can result in a broken null cycle instead (Blokhuys et al., 2025). The Chapman mechanism (Chapman, 1932), with 4 species of interest and 5 reactions, has one instance of coproduction: reactions (R3) and (R4). See the below set of reactions, and the matrices in Figure S1.

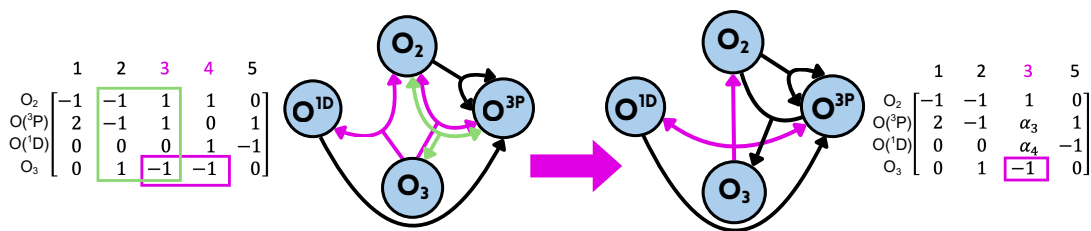
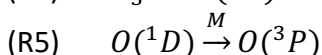
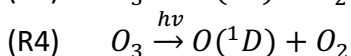
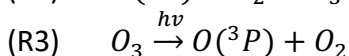
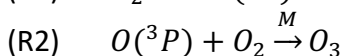
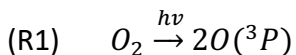
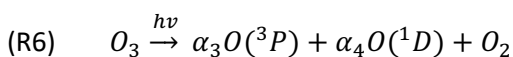


Figure S1. A broken null cycle from coproduction in the Chapman mechanism

(M1) is the stoichiometric matrix of the Chapman mechanism, and (M2) is the result of merging reactions (R3) and (R4). Following the merging procedure, we see that $O(^3P)$ and $O(^1D)$ are produced at the fractional kinetic rates α_3 and α_4 respectively.

$$(M1) \quad \begin{matrix} O_2 \\ O(^3P) \\ O(^1D) \\ O_3 \end{matrix} \begin{bmatrix} -1 & -1 & 1 & 1 & 0 \\ 2 & -1 & 1 & 0 & 1 \\ 0 & 0 & 0 & 1 & -1 \\ 0 & 1 & -1 & -1 & 0 \end{bmatrix} \Rightarrow (M2) \quad \begin{matrix} O_2 \\ O(^3P) \\ O(^1D) \\ O_3 \end{matrix} \begin{bmatrix} -1 & -1 & 1 & 0 \\ 2 & -1 & \alpha_3 & 1 \\ 0 & 0 & \alpha_4 & -1 \\ 0 & 1 & -1 & 0 \end{bmatrix}$$

The newly merged reaction can be written as

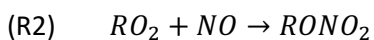
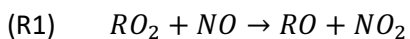


Notice that (R2) and (R3) together make up a null cycle (the net change of the respective participating species is zero when both reactions occur simultaneously). However, (R3) also participates in coproduction. One unit of $O(^3P)$ reacts with O_2 in (R2) to complete the production of ozone for consumption in (R3), but because of coproduction, only α_3 -amount of $O(^3P)$ is produced and available to react at a time, hence the disruption of the null cycle. From a linear algebra perspective, the emergent invariant is usually identified by a reduction in rank from (M1) to (M2). But null cycles create a set of linearly dependent vectors that prevent the matrix from

being full-rank in the first place. Breaking the null cycle cancels out the rank-reduction effect of merging and thus doesn't lead to the appearance of an emergent invariant. The merged matrix (M2) (also depicted on the right side of Figure S1) helps us visualize the loss of the cycle. The ranks of both (M1) and (M2) can be verified to be the same – both equal to 3.

Text S2. RO₂+NO branching reactions example: deriving a kinetic invariant and a reduced system with identical behavior

The following section demonstrates how a kinetic invariant emerges in a small chemical system (RO₂+NO branching reactions), and how invariants constrain the space in which this chemical system evolves. We start with 5 species of interest interacting in 3 reactions:



By the law of mass action, the reaction rates are proportional to the product of the concentrations of the co-reactants via rate constant proportionalities k_1, k_2, k_3 , respectively. The rates of change

of each species can then be determined by which reactions it is consumed or produced in. For example, RO_2 is consumed in R1 and R2, and produced in R3:

I. RO_2 is consumed at the rate $k_1[RO_2][NO]$ in R1

II. RO_2 is consumed at the rate $k_2[RO_2][NO]$ in R2

III. RO_2 is produced at the rate $k_3[RO]$ in R3

Hence we obtain

$$(E1) \quad d_t[RO_2] = -k_1[RO_2][NO] - k_2[RO_2][NO] + k_3[RO]$$

For the remaining 4 species in the system, we follow the same procedure to get:

$$(E2) \quad d_t[NO] = -k_1[RO_2][NO] - k_2[RO_2][NO]$$

$$(E3) \quad d_t[RO] = k_1[RO_2][NO] - k_3[RO]$$

$$(E4) \quad d_t[NO_2] = k_1[RO_2][NO]$$

$$(E5) \quad d_t[RONO_2] = k_2[RO_2][NO]$$

The species in the system are chemical combinations of the elements O and N, and the R group. As written, the overall concentrations of R and N are conserved within the system because of the mass balance (the balance of oxygen is not tracked), producing 2 conservation laws L_1 and L_2 :

$$L_1 = [RO_2] + [RO] + [RONO_2], \quad \text{summing the concentrations of R-containing species}$$

$$L_2 = [NO_2] + [NO] + [RONO_2], \quad \text{summing the concentrations of N-containing species}$$

The original system can be represented as a stoichiometric matrix (M1), with each row corresponding to species and each column corresponding to reactions. Notice that columns 1 and 2 have the same reactant species, i.e. a pair of branching reactions. These reactions can be “merged” within the matrix, with the original stoichiometric coefficients replaced by $\alpha_1 = \frac{k_1}{k_1+k_2}$ and $\alpha_2 = 1 - \frac{k_1}{k_1+k_2} = \frac{k_2}{k_1+k_2}$ for species produced in reaction 1 and reaction 2 at new fractional

kinetic rates α_1 and α_2 respectively. The newly merged effective reaction (R4) is shown in the matrix (M2) below and proceeds at a rate of $(k_1 + k_2) [RO_2][NO]$.



$$(M1) \begin{matrix} RO_2 \\ RO \\ NO \\ NO_2 \\ RONO_2 \end{matrix} \begin{bmatrix} -1 & -1 & 1 \\ 1 & 0 & -1 \\ -1 & -1 & 0 \\ 1 & 0 & 0 \\ 0 & 1 & 0 \end{bmatrix} \rightarrow (M2) \begin{matrix} RO_2 \\ RO \\ NO \\ NO_2 \\ RONO_2 \end{matrix} \begin{bmatrix} -1 & 1 \\ \alpha_1 & -1 \\ -1 & 0 \\ \alpha_1 & 0 \\ \alpha_2 & 0 \end{bmatrix}$$

The kinetics of the branching reactions in this system lead to an emergent conserved property, a kinetic invariant L_3 . This arises because products of the two merged reactions, NO_2 and $RONO_2$, are linked and kinetically proportional. Taking the rates of change of the products in (E4) and (E5) and rearranging, we obtain

$$(E6) \quad [RO_2][NO] = \frac{d_t[NO_2]}{k_1}$$

$$(E7) \quad [RO_2][NO] = \frac{d_t[RONO_2]}{k_2}$$

Equating the R.H.S. we obtain $\frac{d_t[NO_2]}{k_1} = \frac{d_t[RONO_2]}{k_2}$, or $k_2 * d_t[NO_2] = k_1 * d_t[RONO_2]$. Rearranging and integrating results in the kinetic invariant:

$$L_3 = k_2[NO_2] - k_1[RONO_2]$$

L_3 is constant under constant environmental conditions, as it is a function of rate constants which in turn are dependent on temperature (outside of this example, rate constants can be dependent on other environmental conditions: effective-second-order rate constants for termolecular reactions are also dependent on pressure, and photolytic rate constants are a function of actinic flux). In general, kinetic invariants can emerge in situations where environmental conditions are held constant but chemical conditions can still be rapidly evolving, such as a chemistry operator step in a 3D atmospheric model, or in a controlled chamber experiment.

With the new conservation law L_3 , we can now reduce the dimensionality of the original system. In other words, as opposed to tracking the concentration of all species, it is possible to only track

that of 2 out of 5 species and use the 3 conservation laws to determine the concentrations of the rest.

Returning to the definitions of L_1 , L_2 , and L_3 , we can represent this system of 3 equations in matrix form:

$$(E8) \quad \begin{bmatrix} 1 & 1 & 0 & 0 & 1 \\ 0 & 0 & 1 & 1 & 1 \\ 0 & 0 & 0 & k_2 & -k_1 \end{bmatrix} \begin{bmatrix} RO_2 \\ RO \\ NO \\ NO_2 \\ RONO_2 \end{bmatrix} = \begin{bmatrix} L_1 \\ L_2 \\ L_3 \end{bmatrix}$$

We label the first L.H.S. matrix as M^T (where M would be the matrix form of the 3 conservation laws). The second L.H.S. matrix we call C , the matrix of concentration values for each species.

$$(E9) \quad M^T C = L = \begin{bmatrix} L_1 \\ L_2 \\ L_3 \end{bmatrix}$$

We can look at M^T as a combination of two matrices M_{free} and M_{dep} , determined by which species have concentrations that are dependent on or constrained by chemical kinetics. We

choose $[RO_2]$, $[RO]$ to be the “free” species (though this is not the only combination of species that can be chosen to be free).

$$(E10) \quad M^T = [M_{free}|M_{dep}]$$

$$(E11) \quad [M_{free}|zeros] \begin{bmatrix} RO_2 \\ RO \\ NO \\ NO_2 \\ RONO_2 \end{bmatrix} + [zeros|M_{dep}] \begin{bmatrix} RO_2 \\ RO \\ NO \\ NO_2 \\ RONO_2 \end{bmatrix} = \begin{bmatrix} L_1 \\ L_2 \\ L_3 \end{bmatrix}$$

$$(E12) \quad M_{free} \begin{bmatrix} RO_2 \\ RO \end{bmatrix} + M_{dep} \begin{bmatrix} NO \\ NO_2 \\ RONO_2 \end{bmatrix} = L$$

Using linear algebra, we isolate and solve for $\begin{bmatrix} NO \\ NO_2 \\ RONO_2 \end{bmatrix}$ from (E12) by subtracting $M_{free} \begin{bmatrix} RO_2 \\ RO \end{bmatrix}$ from L and multiplying the difference by the inverse of M_{dep} :

$$(E13) \quad \begin{bmatrix} NO \\ NO_2 \\ RONO_2 \end{bmatrix} = M_{dep}^{-1} (L - M_{free} \begin{bmatrix} RO_2 \\ RO \end{bmatrix})$$

We rearrange L_1 , L_2 , and L_3 :

$$(E14) \quad [RONO_2] = L_1 - [RO_2] - [RO]$$

$$(E15) \quad [NO] = L_2 - [NO_2] - [RONO_2]$$

$$(E16) \quad [NO_2] = \frac{L_3 + k_1 [RONO_2]}{k_2}$$

We can rewrite the rearranged conservation law equations to be in terms of only the free species, chosen to be RO_2 and RO . We substitute $[RONO_2]$ in (E16) with the R.H.S. of (E14) to get:

$$(E17) \quad [NO_2] = \frac{L_3 + k_1 (L_1 - [RO_2] - [RO])}{k_2}$$

Substituting (E17)'s R.H.S. into $[NO_2]$, and (E14)'s R.H.S. into $[RONO_2]$ in (E15) produces:

$$(E18) \quad [NO] = L_2 - \frac{L_3 + k_1 (L_1 - [RO_2] - [RO])}{k_2} - (L_1 - [RO_2] - [RO])$$

Now we perform algebraic substitutions and transformations to reduce the system of equations.

From (E1) we have:

$$d_t [RO_2] = -k_1 [RO_2] [NO] - k_2 [RO_2] [NO] + k_3 [RO]$$

$$d_t[RO_2] = -(k_1 + k_2)[RO_2][NO] + k_3[RO]$$

We substitute the R.H.S. of (E18) into [NO]:

$$d_t[RO_2] = -(k_1 + k_2)[RO_2](L_2 - \frac{L_3 + k_1(L_1 - [RO_2] - [RO])}{k_2} - (L_1 - [RO_2] - [RO])) + k_3[RO]$$

$$d_t[RO_2] = -(k_1 + k_2)[RO_2](L_2 - \frac{L_3}{k_2} - (\frac{k_1 + k_2}{k_2})L_1) - (k_1 + k_2)[RO_2](\frac{k_1 + k_2}{k_2})([RO_2] + [RO]) + k_3[RO]$$

$$d_t[RO_2] = -\frac{(k_1 + k_2)^2}{k_2}[RO_2]^2 - \frac{(k_1 + k_2)^2}{k_2}[RO_2][RO] - (\frac{k_1 + k_2}{k_2})(k_2L_2 - L_3 - (k_1 + k_2)L_1)[RO_2] + k_3[RO]$$

From (E3) we have:

$$d_t[RO] = k_1[RO_2][NO] - k_3[RO]$$

Similarly, we substitute [NO]:

$$d_t[RO] = k_1[RO_2](L_2 - \frac{L_3 + k_1(L_1 - [RO_2] - [RO])}{k_2} - (L_1 - [RO_2] - [RO])) - k_3[RO]$$

$$d_t[RO] = k_1[RO_2](L_2 - \frac{L_3}{k_2} - \frac{k_1(L_1)}{k_2} + \frac{k_1[RO_2]}{k_2} + \frac{k_1[RO]}{k_2} - (L_1 - [RO_2] - [RO])) - k_3[RO]$$

$$d_t[RO] = k_1[RO_2](L_2 - \frac{L_3}{k_2} - L_1 \frac{k_1 + k_2}{k_2} + [RO_2] \frac{k_1 + k_2}{k_2} + [RO] \frac{k_1 + k_2}{k_2}) - k_3[RO]$$

$$d_t[RO] = \frac{k_1(k_1 + k_2)}{k_2}[RO_2]^2 + \frac{k_1(k_1 + k_2)}{k_2}[RO_2][RO] + (\frac{k_1}{k_2})(k_2L_2 - L_3 - (k_1 + k_2)L_1)[RO] - k_3[RO]$$

We end up with the following two differential equations, reducing the system of originally 5 dimensions to only 2.

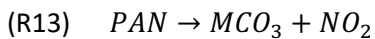
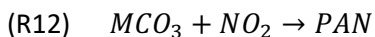
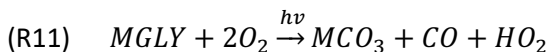
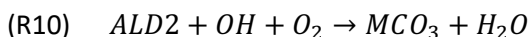
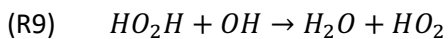
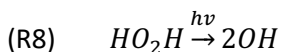
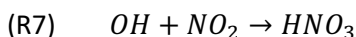
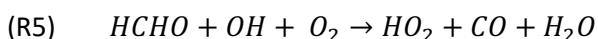
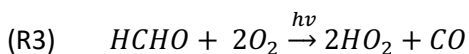
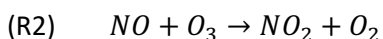
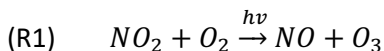
$$d_t[RO_2] = -\frac{(k_1 + k_2)^2}{k_2}[RO_2]^2 - \frac{(k_1 + k_2)^2}{k_2}[RO_2][RO] - (\frac{k_1 + k_2}{k_2})(k_2L_2 - L_3 - (k_1 + k_2)L_1)[RO_2] + k_3[RO]$$

$$d_t[RO] = \frac{k_1(k_1 + k_2)}{k_2} [RO_2]^2 + \frac{k_1(k_1 + k_2)}{k_2} [RO_2][RO] + \left(\frac{k_1}{k_2}\right)(k_2L_2 - L_3 - (k_1 + k_2)L_1)[RO_2] - k_3[RO]$$

This 2-dimensional ODE system evolves in exactly the same way as the 5-dimensional ODE system, under fixed environmental conditions. In other words, the system of 5 species evolves on a 2D manifold within a 5D space. Given the constants L_1 , L_2 and L_3 , the concentrations of the 3 other species can be reconstructed from $[RO_2]$ and $[RO]$ at any point.

Text S3. Derivation of the kinetic invariant in the Julia photochemical mechanism

This section demonstrates how a kinetic invariant emerges in the Julia Photochemical Mechanism (JPM v1.1), following similar mathematical procedures as that of the example RO_2 mechanism. We start with 16 species of interest interacting in 13 reactions:



Note that O_2 has been added to track oxygen conservation, though it does not participate as an explicit factor in the otherwise mass-action rate laws. The JPM mechanism can be represented as

a stoichiometric matrix (M1), with rows corresponding to species and columns corresponding to reactions.

(M1)

<i>spc</i>	R1	R2	R3	R4	R5	R6	R7	R8	R9	R10	R11	R12	R13
O_3	1	-1	0	0	0	0	0	0	0	0	0	0	0
NO	1	-1	0	0	0	-1	0	0	0	0	0	0	0
NO_2	-1	1	0	0	0	1	-1	0	0	0	0	-1	1
$HCHO$	0	0	-1	-1	-1	0	0	0	0	0	0	0	0
HO_2	0	0	2	0	1	-1	0	0	1	0	1	0	0
H_2O_2	0	0	0	0	0	0	0	-1	-1	0	0	0	0
OH	0	0	0	0	-1	1	-1	2	-1	-1	0	0	0
HNO_3	0	0	0	0	0	0	1	0	0	0	0	0	0
CO	0	0	1	1	1	0	0	0	0	0	1	0	0
H_2	0	0	0	1	0	0	0	0	0	0	0	0	0
$ALD2$	0	0	0	0	0	0	0	0	0	-1	0	0	0
$MGLY$	0	0	0	0	0	0	0	0	0	0	-1	0	0
MCO_3	0	0	0	0	0	0	0	0	0	1	1	-1	1
PAN	0	0	0	0	0	0	0	0	0	0	0	1	-1
H_2O	0	0	0	0	1	0	0	0	1	1	0	0	0
O_2	-1	1	-2	0	-1	0	0	0	0	-1	-2	0	0

By construction, this mechanism conserves the atoms of 4 elements: *C*, *H*, *N*, and *O*. Thus we have 4 initial conservation laws.

$$L_C = [HCHO] + [CO] + 2[ALD2] + 3[MGLY] + 2[MCO_3] + 2[PAN]$$

$$L_N = [NO] + [NO_2] + [HNO_3] + [PAN]$$

$$L_H = 2[HCHO] + [HO_2] + 2[H_2O_2] + [OH] + [HNO_3] + 2[H_2] + 4[ALD2] + 4[MGLY] + 3[MCO_3] +$$

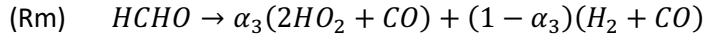
$$3[PAN] + 2[H_2O]$$

$$L_O = 3[O_3] + [NO] + 2[NO_2] + [HCHO] + 2[HO_2] + 2[H_2O_2] + [OH] + 3[HNO_3] + [CO] + [ALD2] +$$

$$2[MGLY] + 3[MCO_3] + 5[PAN] + [H_2O] + 2[O_2]$$

L_C , L_N , L_H , L_O correspond to carbon, nitrogen, hydrogen, and oxygen conservation respectively. These stoichiometric invariants (i.e. structural invariants from atom conservation that exist

stoichiometric coefficients are replaced by $\alpha_3 = \frac{k_3}{k_3+k_4}$ and $\alpha_4 = 1 - \frac{k_3}{k_3+k_4} = \frac{k_4}{k_3+k_4}$ for species produced in (R3) and (R4) at new branching ratios α_3 and α_4 respectively.



(M₂)

spc	R1	R2	Rm	R5	R6	R7	R8	R9	R10	R11	R12	R13
O ₃	1	-1	0	0	0	0	0	0	0	0	0	0
NO	1	-1	0	0	-1	0	0	0	0	0	0	0
NO ₂	-1	1	0	0	1	-1	0	0	0	0	-1	1
HCHO	0	0	-1	-1	0	0	0	0	0	0	0	0
HO ₂	0	0	2α ₃	1	-1	0	0	1	0	1	0	0
H ₂ O ₂	0	0	0	0	0	0	-1	-1	0	0	0	0
OH	0	0	0	-1	1	-1	2	-1	-1	0	0	0
HNO ₃	0	0	0	0	0	1	0	0	0	0	0	0
CO	0	0	α ₃ + α ₄	1	0	0	0	0	0	1	0	0
H ₂	0	0	α ₄	0	0	0	0	0	0	0	0	0
ALD2	0	0	0	0	0	0	0	0	-1	0	0	0
MGLY	0	0	0	0	0	0	0	0	0	-1	0	0
MCO ₃	0	0	0	0	0	0	0	0	1	1	-1	1
PAN	0	0	0	0	0	0	0	0	0	0	1	-1
H ₂ O	0	0	0	1	0	0	0	1	1	0	0	0
O ₂	-1	1	-2α ₃	-1	0	0	0	0	-1	-2	0	0

Since *CO* appears as a product in both (R3) and (R4), it is produced in (Rm) with a stoichiometric weight of (α₃ + α₄), which equals 1.

As in the example of the *RO₂ + NO* branching reactions, the kinetic proportionality of the products of the branching reactions lead to an emergent kinetic invariant $L_{kinetic}$. Note that all stoichiometric and kinetic invariants exist in the mechanism before *and* after merging. The merging operation simply allows us to visualize these conservation laws in a more mathematically interpretable way. The JPM mechanism is larger than the *RO₂* mechanism, hence finding $L_{kinetic}$ requires a longer algebraic approach. The overall change in concentration of each species can be written as a sum of the rates of the reactions they participate in. For example, *O₃* is produced in

(R1) and consumed in (R2), so the instantaneous time rate of change of O_3 concentration can be written as $d_t[O_3] = r_1 - r_2$, where r_1 and r_2 denote the reaction rates of R1 and R2 respectively.

$$d_t[O_3] = r_1 - r_2$$

$$d_t[NO] = r_1 - r_2 - r_6$$

$$d_t[HO_2] = 2r_3 + r_5 - r_6 + r_9 + r_{11}$$

$$d_t[H_2] = r_4$$

$$d_t[ALD2] = -r_{10}$$

$$d_t[MGLY] = -r_{11}$$

$$d_t[H_2O] = r_5 + r_9 + r_{10}$$

After the merging of (R3) and (R4) into (R_m), we can represent the rates of R3 and R4 as $(\alpha_3 r_m)$ and $(\alpha_4 r_m)$ respectively, affecting only $d_t[HO_2]$ and $d_t[H_2]$.

$$d_t[HO_2] = 2\alpha_3 r_m + r_5 - r_6 + r_9 + r_{11}$$

$$d_t[H_2] = \alpha_4 r_m$$

Now we attempt to manually find a vector that fulfills two requirements: 1) it lies in the null space of M_2 and 2) it is not already part of the null space of M_1 . In other words, we want to find a combination of the 7 equations corresponding to species rates that result in net zero change

overall. We also aim to make each element of the vector a multiple of α_3 or α_4 to satisfy requirement (2). We arrive at the following solution:

$$\alpha_4 * d_t[O_3] = \alpha_4 r_1 - \alpha_4 r_2$$

$$-\alpha_4 * d_t[NO] = -\alpha_4 r_1 + \alpha_4 r_2 + \alpha_4 r_6$$

$$\alpha_4 * d_t[HO_2] = 2\alpha_3 \alpha_4 r_m + \alpha_4 r_5 - \alpha_4 r_6 + \alpha_4 r_9 + \alpha_4 r_{11}$$

$$-2\alpha_3 * d_t[H_2] = -2\alpha_3 \alpha_4 r_m$$

$$-\alpha_4 * d_t[ALD2] = \alpha_4 r_{10}$$

$$\alpha_4 * d_t[MGLY] = -\alpha_4 r_{11}$$

$$-\alpha_4 * d_t[H_2O] = -\alpha_4 r_5 - \alpha_4 r_9 - \alpha_4 r_{10}$$

This results in the vector v_1

$$v_1 = \begin{bmatrix} \alpha_4 \\ -\alpha_4 \\ 0 \\ 0 \\ \alpha_4 \\ 0 \\ 0 \\ 0 \\ 0 \\ -2\alpha_3 \\ -\alpha_4 \\ 0 \\ -\alpha_4 \\ \alpha_4 \\ 0 \\ 0 \end{bmatrix}$$

corresponding to the kinetic invariant

$$0 = \alpha_4 d_t[O_3] - \alpha_4 d_t[NO] + \alpha_4 d_t[HO_2] - 2\alpha_3 d_t[H_2] - \alpha_4 d_t[ALD2] + \alpha_4 d_t[MGLY] - \alpha_4 d_t[H_2O]$$

Which when integrated is equal to a constant in time:

$$L_{kinetic} = \alpha_4 [O_3] - \alpha_4 [NO] + \alpha_4 [HO_2] - 2\alpha_3 [H_2] - \alpha_4 [ALD2] + \alpha_4 [MGLY] - \alpha_4 [H_2O]$$

We can verify that adding up all the R.H.S. of the equations with coefficients equals 0. Additionally, performing the matrix operation $v_1^T M_2$ results in the null (zero) vector. Finally, we recognize that v_1 is linearly independent of the 5 stoichiometric conservation laws $[M_L | L_{subpool}]$

It is worth noting that, if obtained via other methods, the set of 6 vectors corresponding to the conservation laws might not be the same as our findings. We wanted to see if our analytical

solution would produce the same results as a data-driven version, hence we performed the PCA method mentioned in Section 3 of the main text. As shown in Figure 2, the data-driven results do agree with the analytical ones in terms of the number of invariants overall. However, the data-driven vectors do not correspond directly to each of the conservation laws we analytically derived. Instead, the data-driven eigenvectors form a linear basis for the analytically-derived conservation laws.

Text S4. Survey of dimensionality in various chemical mechanisms

For larger mechanisms, symbolic nullspaces can become extremely costly to compute. To calculate dimensionality of these mechanisms, we instead run numerical computations where rate constants are assigned numerical values for each mechanism, using 10 independently randomized trials – we find that the numerical experiments are robust to random assignment and always give identical values every time. For mechanisms like the MCM with a huge number of reactions, we make additional adjustments to the dimensional computation algorithm for the sake of computational feasibility. MCM’s reaction (column) space is much larger than its species (row) space, so for each experiment iteration, we perform “randomized sketching”. We project the stoichiometric matrix onto a full-rank, random Gaussian square matrix of the same dimension as the species space. By collapsing the column space, we can perform the numerical rank calculations for very large mechanisms like MCM within reasonable timeframes and without sacrificing validity. See Table S1 and Figure S2 for all mechanisms in the survey.

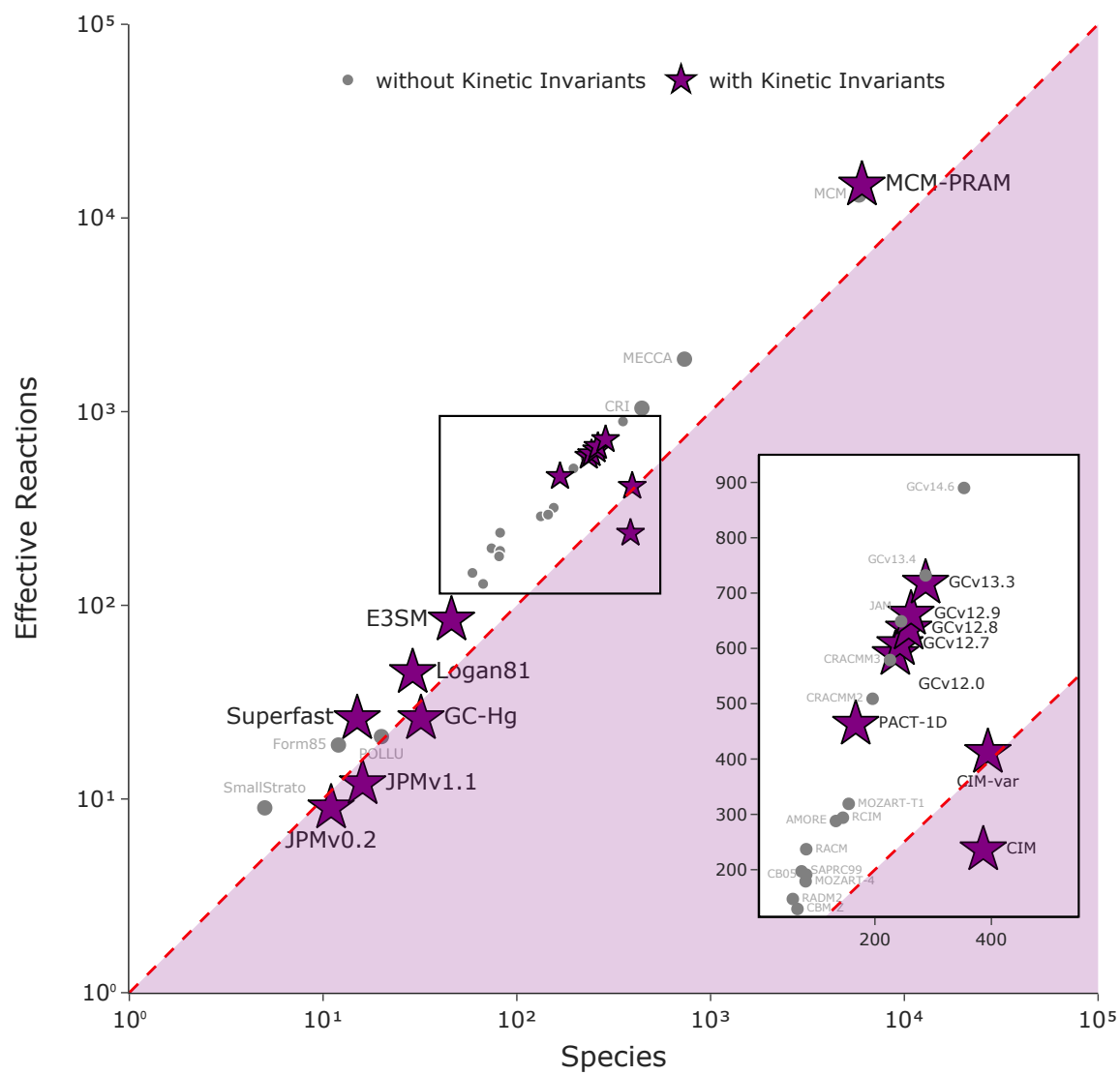


Figure S2. Log-scale version of Figure 3, containing all 35 mechanisms in the survey

Table S1. Survey of emergent conservation in 35 chemical mechanisms

Mechanism	Short Name	Species	Reactions	Stoichiometric Invariants	Largest Merged Group	# Merged Groups	Coproduct Index	Kinetic Invariants	Broken Null Cycles	References and Source Notes
Small Strato	SmallStrato	5	10	1	2	1	1	0	1	(Damian et al., 2002)
Julia Photochem v0.2	JPMv0.2	11	10	2	2	1	1	1	0	(Sturm & Wexler, 2022)
Julia Photochem v1.1	JPMv1.1	16	13	5	2	1	1	1	0	(Sturm & Silva, 2024)
Form8S	Form8S	12	25	1	3	5	6	0	6	(Vajda et al., 1985) is the first obtainable reference
Superfast	Superfast	15	32	0	3	5	6	1	5	Original reference (Cameron-Smith et al., 2006), obtained in KPP format from (Kelp et al., 2022) and added sulfate chem back based on table S2 of the supplement of (Brown-Steiner et al., 2018)
Verwer1994 (POLLU)	POLLU	20	25	3	2	4	4	0	4	(Verwer, 1994) is the first obtainable reference
Logan1981	Logan81	29	54	3	3	8	9	1	8	(Logan et al., 1981) table 1, gas-phase mechanism reactions 1-49. Note that we expand branching reaction and reversible reactions as their own reactions, leading to a higher count of overall reactions. The original paper used an O1D quantum yield of unity (100%) from O3 photolysis in reaction 40, which we preserve.
GEOS-Chem Hg	GC-Hg	32	91	2	11	24	65	4	61	(Shah et al., 2021), exact KPP version downloaded as part of GC14.6.3: https://doi.org/10.5281/zenodo.1653868 ; 3 null reactions not included in reaction count.
E3SM-chem	E3SM	46	103	1	3	15	19	1	18	(Tang et al., 2025) obtained from data availability statement https://github.com/E3SM-Project/E3SM/blob/master/components/eam/src/chemistry/go_chemuci/linux2_mam5_vbs/chem_mech.in , last access February 12, 2026; 1 null reaction not included in reaction count.
CBM-Z	CBM-Z	67	139	7	3	9	10	0	10	(Zaveri & Peters, 1999), * - 3 null reactions not included in reaction count.
RADM2	RADM2	59	156	2	2	9	9	0	9	(Stockwell et al., 1990),*
SAPRC99	SAPRC99	74	210	1	2	13	13	0	13	(Carter, 2000), part of KPP software examples (Damian et al., 2002; Lin et al., 2023); 1 null reaction not included in reaction count.
CB05-TUCI	CB05	82	205	7	4	12	14	0	14	(Whitten et al., 2010),*
RACM	RACM	82	250	1	2	13	13	0	13	(Stockwell et al., 1997)
CRACMM2	CRACMM2	196	531	4	4	16	22	0	22	(Pye et al., 2023; Skipper et al., 2024)
CRACMM3	CRACMM3	226	614	5	4	23	35	0	35	Downloaded from the CRACMM Repo Update Oct 2025: https://doi.org/10.23719/d-1dx . Note: adding the eliminated element tracking species adds 3 species, but only 1 additional stoichiometric invariant, indicating that 2 of 3 of the balance species do not close the atom balance
MOZART-4	MOZART-4	81	196	0	3	16	17	0	17	(Emmons et al., 2010),*
MOZART-T1	MOZART-T1	155	360	0	3	39	41	0	41	(Emmons et al., 2020),*
AMORE-Isoprene v2.0, 109 isoprene-derived species	AMORE	133	330	0	4	32	42	0	42	(Wiser et al., 2025) downloaded from https://doi.org/10.5281/zenodo.15026991 (Wiser et al., 2025) found that the 133-species AMORE-isoprene mechanism had better fidelity compared to CIM than its comparable size RCIM (pink vs orange points in Figure 2 and Figure 3b of Wiser et al. (2025) – note the number of species discrepancy is because the number in the reference includes only isoprene-derived species). As neither AMORE-isoprene nor RCIM has stoichiometric invariants or emergent conservation from kinetic invariants, neither has an effective dimensionality lower than its respective number of species. Reduced intrinsic dimensionality from emergent conservation can be ruled out as a structural cause of the difference in fidelity between RCIM and its comparatively sized AMORE-isoprene mechanism.
PACT-1D-HALOGENS-v1.1	PACT-1D	167	512	9	4	36	49	1	48	(Ahmed et al., 2022) and Zenodo https://doi.org/10.5281/zenodo.6045999 ; 1 null reaction not included in reaction count.
Caltech reduced plus v5	RCIM	145	379	0	5	64	85	0	85	(Wennberg et al., 2018) downloaded from (Bates & Wennberg, 2017)
Caltech Isoprene Mechanism Full v5	CIM	386	886	0	15	195	650	150	500	(Wennberg et al., 2018) downloaded from (Bates & Wennberg, 2017)
Caltech Isoprene Mechanism, Variable Oxidants	CIM-var	394	886	2	8	284	474	17	457	(Wennberg et al., 2018) downloaded from (Bates & Wennberg, 2017)
Jülich Atmospheric Mechanism JAM002b	JAM	245	702	4	4	41	53	0	53	(Schultz et al., 2018) downloaded in the supplement of (Sander, 2024)
GEOS-Chem v12.0.0	GCv12.0	235	725	6	6	101	136	1	135	Standard mechanism downloaded from https://doi.org/10.5281/zenodo.1343547
GEOS-Chem v12.7.0	GCv12.7	243	750	6	6	108	143	1	142	Standard mechanism downloaded from https://doi.org/10.5281/zenodo.3634864
GEOS-Chem v12.8.0	GCv12.8	258	825	6	6	138	190	1	189	Standard mechanism downloaded from https://doi.org/10.5281/zenodo.3784796
GEOS-Chem v12.9.0	GCv12.9	262	850	8	6	138	188	2	186	Standard mechanism downloaded from https://doi.org/10.5281/zenodo.3950327 . Ablation study with no P/L species showed the mechanism still has 2 kinetic invariants
GEOS-Chem v13.3.0	GCv13.3	287	903	10	6	140	185	2	183	Full chem mechanism downloaded from https://doi.org/10.5281/zenodo.7254231
GEOS-Chem v13.4.0	GCv13.4	287	913	10	6	138	181	0	181	Full chem mechanism downloaded from https://doi.org/10.5281/zenodo.7254268
GEOS-Chem v14.6.3	GCv14.6	353	1058	9	5	123	168	0	168	Full chem mechanism downloaded from https://doi.org/10.5281/zenodo.1653868
CRI v2.2	CRI	442	1258	2	6	179	216	0	216	(Jenkin et al., 2008, 2019; Watson et al., 2008) downloaded from https://www.mcm.york.ac.uk/CRI/ last access November 6, 2025.
CAABA/MECCA v4.6.0	MECCA	733	2323	9	8	361	456	0	456	Downloaded as gas.kpp mechanism in the supplement of (Sander, 2024). The most recent code is available on gitlab: https://gitlab.com/RolfSander/caaba-mecca
MCM v3.3.1	MCM	5832	16698	1	7	2617	3558	0	3558	(Bloss et al., 2005; Jenkin et al., 1997, 2012, 2015; Saunders et al., 2003) downloaded from https://www.mcm.york.ac.uk/MCM/ last access November 6, 2025.
MCM with PRAM	MCM-PRAM	6041	18478	1	7	2654	3671	3	3668	MCM v3.3.1 as above, paired with PRAM downloaded in KPP format (Roldin, 2019; Roldin et al., 2019)

*downloaded in KPP format from the BOXMOX (Knote et al., 2015) repository: https://mbees.med.uni-augsburg.de/gitlab/mbees/boxmox/-/tree/master/models?ref_type=heads, last access January 6, 2025

1 References

- 2 Ahmed, S., Thomas, J. L., Tuite, K., Stutz, J., Flocke, F., Orlando, J. J., et al. (2022). The Role of Snow in Controlling Halogen
3 Chemistry and Boundary Layer Oxidation During Arctic Spring: A 1D Modeling Case Study. *Journal of Geophysical*
4 *Research: Atmospheres*, 127(5), e2021JD036140. <https://doi.org/10.1029/2021JD036140>
- 5 Bates, K., & Wennberg, P. (2017). Isoprene Oxidation Model. Retrieved from <https://data.caltech.edu/records/x88rk-wca37>
- 6 Blokhuis, A., Kuppeveld, M. van, Weem, D. van de, & Pollice, R. (2025, June 15). On data and dimension in chemistry --
7 irreversibility, concealment and emergent conservation laws. arXiv. <https://doi.org/10.48550/arXiv.2306.09553>
- 8 Bloss, C., Wagner, V., Jenkin, M. E., Volkamer, R., Bloss, W. J., Lee, J. D., et al. (2005). Development of a detailed chemical
9 mechanism (MCMv3.1) for the atmospheric oxidation of aromatic hydrocarbons. *Atmospheric Chemistry and Physics*,
10 5(3), 641–664. <https://doi.org/10.5194/acp-5-641-2005>
- 11 Brown-Steiner, B., Selin, N. E., Prinn, R., Tilmes, S., Emmons, L., Lamarque, J.-F., & Cameron-Smith, P. (2018). Evaluating
12 simplified chemical mechanisms within present-day simulations of the Community Earth System Model version 1.2
13 with CAM4 (CESM1.2 CAM-chem): MOZART-4 vs. Reduced Hydrocarbon vs. Super-Fast chemistry. *Geoscientific Model*
14 *Development*, 11(10), 4155–4174. <https://doi.org/10.5194/gmd-11-4155-2018>
- 15 Cameron-Smith, P., Lamarque, J.-F., Connell, P., Chuang, C., & Vitt, F. (2006). Toward an Earth system model: atmospheric
16 chemistry, coupling, and petascale computing. *Journal of Physics: Conference Series*, 46(1), 343.
17 <https://doi.org/10.1088/1742-6596/46/1/048>
- 18 Carter, W. P. L. (2000). Documentation for the SAPRC-99 Chemical Mechanism And Updated VOC Reactivity Scales. Retrieved
19 February 12, 2026, from <https://intra.engr.ucr.edu/~carter/reactdat.htm>
- 20 Chapman, S. (1932). Discussion of memoirs. On a theory of upper-atmospheric ozone. *Quarterly Journal of the Royal*
21 *Meteorological Society*, 58(243), 11–13. <https://doi.org/10.1002/qj.49705824304>
- 22 Damian, V., Sandu, A., Damian, M., Potra, F., & Carmichael, G. R. (2002). The kinetic preprocessor KPP-a software environment
23 for solving chemical kinetics. *Computers & Chemical Engineering*, 26(11), 1567–1579. <https://doi.org/10.1016/S0098->
24 1354(02)00128-X
- 25 Emmons, L. K., Schwantes, R. H., Orlando, J. J., Tyndall, G., Kinnison, D., Lamarque, J.-F., et al. (2020). The Chemistry Mechanism
26 in the Community Earth System Model Version 2 (CESM2). *Journal of Advances in Modeling Earth Systems*, 12(4),
27 e2019MS001882. <https://doi.org/10.1029/2019MS001882>
- 28 Emmons, Louisa. K., Walters, S., Hess, P. G., Lamarque, J.-F., Pfister, G. G., Fillmore, D., et al. (2010). Description and evaluation
29 of the Model for Ozone and Related chemical Tracers, version 4 (MOZART-4). *Geoscientific Model Development*, 3(1),
30 43–67. <https://doi.org/10.5194/gmd-3-43-2010>
- 31 Jenkin, M. E., Saunders, S. M., & Pilling, M. J. (1997). The tropospheric degradation of volatile organic compounds: a protocol
32 for mechanism development. *Atmospheric Environment*, 31(1), 81–104. <https://doi.org/10.1016/S1352->
33 2310(96)00105-7
- 34 Jenkin, M. E., Watson, L. A., Utembe, S. R., & Shallcross, D. E. (2008). A Common Representative Intermediates (CRI) mechanism
35 for VOC degradation. Part 1: Gas phase mechanism development. *Atmospheric Environment*, 42(31), 7185–7195.
36 <https://doi.org/10.1016/j.atmosenv.2008.07.028>
- 37 Jenkin, M. E., Wyche, K. P., Evans, C. J., Carr, T., Monks, P. S., Alfarra, M. R., et al. (2012). Development and chamber evaluation
38 of the MCM v3.2 degradation scheme for β -caryophyllene. *Atmospheric Chemistry and Physics*, 12(11), 5275–5308.
39 <https://doi.org/10.5194/acp-12-5275-2012>
- 40 Jenkin, M. E., Young, J. C., & Rickard, A. R. (2015). The MCM v3.3.1 degradation scheme for isoprene. *Atmospheric Chemistry*
41 *and Physics*, 15(20), 11433–11459. <https://doi.org/10.5194/acp-15-11433-2015>
- 42 Jenkin, M. E., Khan, M. A. H., Shallcross, D. E., Bergström, R., Simpson, D., Murphy, K. L. C., & Rickard, A. R. (2019). The CRI v2.2
43 reduced degradation scheme for isoprene. *Atmospheric Environment*, 212, 172–182.
44 <https://doi.org/10.1016/j.atmosenv.2019.05.055>
- 45 Kelp, M. M., Jacob, D. J., Lin, H., & Sulprizio, M. P. (2022). An Online-Learned Neural Network Chemical Solver for Stable Long-
46 Term Global Simulations of Atmospheric Chemistry. *Journal of Advances in Modeling Earth Systems*, 14(6),
47 e2021MS002926. <https://doi.org/10.1029/2021MS002926>
- 48 Knote, C., Tuccella, P., Curci, G., Emmons, L., Orlando, J. J., Madronich, S., et al. (2015). Influence of the choice of gas-phase
49 mechanism on predictions of key gaseous pollutants during the AQMEII phase-2 intercomparison. *Atmospheric*
50 *Environment*, 115, 553–568. <https://doi.org/10.1016/j.atmosenv.2014.11.066>
- 51 Lin, H., Long, M. S., Sander, R., Sandu, A., Yantosca, R. M., Estrada, L. A., et al. (2023). An Adaptive Auto-Reduction Solver for
52 Speeding Up Integration of Chemical Kinetics in Atmospheric Chemistry Models: Implementation and Evaluation in
53 the Kinetic Pre-Processor (KPP) Version 3.0.0. *Journal of Advances in Modeling Earth Systems*, 15(2), e2022MS003293.
54 <https://doi.org/10.1029/2022MS003293>
- 55 Liu, Z., Sturm, P. O., Bharadwaj, S., Silva, S. J., & Tegmark, M. (2024). Interpretable conservation laws as sparse invariants.
56 *Physical Review E*, 109(2), L023301. <https://doi.org/10.1103/PhysRevE.109.L023301>

57 Logan, J. A., Prather, M. J., Wofsy, S. C., & McElroy, M. B. (1981). Tropospheric chemistry: A global perspective. *Journal of*
58 *Geophysical Research: Oceans*, 86(C8), 7210–7254. <https://doi.org/10.1029/JC086iC08p07210>

59 Pye, H. O. T., Place, B. K., Murphy, B. N., Seltzer, K. M., D'Ambro, E. L., Allen, C., et al. (2023). Linking gas, particulate, and toxic
60 endpoints to air emissions in the Community Regional Atmospheric Chemistry Multiphase Mechanism (CRACMM).
61 *Atmospheric Chemistry and Physics*, 23(9), 5043–5099. <https://doi.org/10.5194/acp-23-5043-2023>

62 Roldin, P. (2019). Peroxy Radical Autoxidation Mechanism (PRAM) [Data set]. *Supplement to: Roldin, Pontus; Ehn, Mikael;*
63 *Kurtén, Theo; Olenius, Tinja; Rissanen, Matti P; Sarnela, Nina; Elm, Jonas; Rantala, Pekka; Hao, Liqing; Hyttinen,*
64 *Noora; Heikkinen, Liine; Worsnop, Douglas R; Pichelstorfer, Lukas; Xavier, Carlton; Clusius, Petri; Öström, Emilie;*
65 *Petäjä, Tuukka; Kulmala, Markku; Vehkamäki, Hanna; Virtanen, Annele; Riipinen, Ilona; Boy, Michael (2019): The role*
66 *of highly oxygenated organic molecules in the Boreal aerosol-cloud-climate system. Nature Communications*, 10(1),
67 <https://doi.org/10.1038/s41467-019-12338-8>. PANGAEA. <https://doi.org/10.1594/PANGAEA.905102>

68 Roldin, P., Ehn, M., Kurtén, T., Olenius, T., Rissanen, M. P., Sarnela, N., et al. (2019). The role of highly oxygenated organic
69 molecules in the Boreal aerosol-cloud-climate system. *Nature Communications*, 10(1), 4370.
70 <https://doi.org/10.1038/s41467-019-12338-8>

71 Sander, R. (2024). MEXPLORER 1.0.0 – a mechanism explorer for analysis and visualization of chemical reaction pathways based
72 on graph theory. *Geoscientific Model Development*, 17(6), 2419–2425. <https://doi.org/10.5194/gmd-17-2419-2024>

73 Saunders, S. M., Jenkin, M. E., Derwent, R. G., & Pilling, M. J. (2003). Protocol for the development of the Master Chemical
74 Mechanism, MCM v3 (Part A): tropospheric degradation of non-aromatic volatile organic compounds. *Atmospheric*
75 *Chemistry and Physics*, 3(1), 161–180. <https://doi.org/10.5194/acp-3-161-2003>

76 Schultz, M. G., Stadler, S., Schröder, S., Taraborrelli, D., Franco, B., Krefting, J., et al. (2018). The chemistry–climate model
77 ECHAM6.3-HAM2.3-MOZ1.0. *Geoscientific Model Development*, 11(5), 1695–1723. [https://doi.org/10.5194/gmd-11-](https://doi.org/10.5194/gmd-11-1695-2018)
78 1695-2018

79 Shah, V., Jacob, D. J., Thackray, C. P., Wang, X., Sunderland, E. M., Dibble, T. S., et al. (2021). Improved Mechanistic Model of the
80 Atmospheric Redox Chemistry of Mercury. *Environmental Science & Technology*, 55(21), 14445–14456.
81 <https://doi.org/10.1021/acs.est.1c03160>

82 Skipper, T. N., D'Ambro, E. L., Wiser, F. C., McNeill, V. F., Schwantes, R. H., Henderson, B. H., et al. (2024). Role of chemical
83 production and depositional losses on formaldehyde in the Community Regional Atmospheric Chemistry Multiphase
84 Mechanism (CRACMM). *Atmospheric Chemistry and Physics*, 24(22), 12903–12924. [https://doi.org/10.5194/acp-24-](https://doi.org/10.5194/acp-24-12903-2024)
85 12903-2024

86 Stockwell, W. R., Middleton, P., Chang, J. S., & Tang, X. (1990). The second generation regional acid deposition model chemical
87 mechanism for regional air quality modeling. *Journal of Geophysical Research: Atmospheres*, 95(D10), 16343–16367.
88 <https://doi.org/10.1029/JD095iD10p16343>

89 Stockwell, W. R., Kirchner, F., Kuhn, M., & Seefeld, S. (1997). A new mechanism for regional atmospheric chemistry modeling.
90 *Journal of Geophysical Research: Atmospheres*, 102(D22), 25847–25879. <https://doi.org/10.1029/97JD00849>

91 Sturm, P. O., & Silva, S. J. (2024). A Nudge to the Truth: Atom Conservation as a Hard Constraint in Models of Atmospheric
92 Composition Using a Species-Weighted Correction. *ACS ES&T Air*. <https://doi.org/10.1021/acsestair.4c00220>

93 Sturm, P. O., & Wexler, A. S. (2022). Conservation laws in a neural network architecture: enforcing the atom balance of a Julia-
94 based photochemical model (v0.2.0). *Geoscientific Model Development*, 15(8), 3417–3431.
95 <https://doi.org/10.5194/gmd-15-3417-2022>

96 Tang, Q., Prather, M. J., Ke, Z., Xie, J., Lee, H.-H., Wu, M., et al. (2025). Interactive Gas Chemistry for Enhanced Science
97 Capabilities of the Energy Exascale Earth System Model Version 3. *Journal of Advances in Modeling Earth Systems*,
98 17(10), e2025MS005062. <https://doi.org/10.1029/2025MS005062>

99 Vajda, S., Valko, P., & Turányi, T. (1985). Principal component analysis of kinetic models. *International Journal of Chemical*
100 *Kinetics*, 17(1), 55–81. <https://doi.org/10.1002/kin.550170107>

101 Verwer, J. G. (1994). Gauss–Seidel Iteration for Stiff ODES from Chemical Kinetics. *SIAM Journal on Scientific Computing*, 15(5),
102 1243–1250. <https://doi.org/10.1137/0915076>

103 Watson, L. A., Shallcross, D. E., Utembe, S. R., & Jenkin, M. E. (2008). A Common Representative Intermediates (CRI) mechanism
104 for VOC degradation. Part 2: Gas phase mechanism reduction. *Atmospheric Environment*, 42(31), 7196–7204.
105 <https://doi.org/10.1016/j.atmosenv.2008.07.034>

106 Wennberg, P. O., Bates, K. H., Crouse, J. D., Dodson, L. G., McVay, R. C., Mertens, L. A., et al. (2018). Gas-Phase Reactions of
107 Isoprene and Its Major Oxidation Products. *Chemical Reviews*, 118(7), 3337–3390.
108 <https://doi.org/10.1021/acs.chemrev.7b00439>

109 Whitten, G. Z., Heo, G., Kimura, Y., McDonald-Buller, E., Allen, D. T., Carter, W. P. L., & Yarwood, G. (2010). A new condensed
110 toluene mechanism for Carbon Bond: CB05-TU. *Atmospheric Environment*, 44(40), 5346–5355.
111 <https://doi.org/10.1016/j.atmosenv.2009.12.029>

112 Wiser, F., Sen, S., Wang, Z., Lee-Taylor, J., Barsanti, K. C., Orlando, J., et al. (2025). A graph theory-based algorithm for the
113 reduction of atmospheric chemical mechanisms. *PNAS Nexus*, 4(9), pgaf273.
114 <https://doi.org/10.1093/pnasnexus/pgaf273>

115 Zaveri, R. A., & Peters, L. K. (1999). A new lumped structure photochemical mechanism for large-scale applications. *Journal of*
116 *Geophysical Research: Atmospheres*, 104(D23), 30387–30415. <https://doi.org/10.1029/1999JD900876>
117

118

119